

# An Optimization Framework for Integrating Electric Vehicles and Carbon Capture: Bridging Cost Gaps via EV deployment

Daniel Fontechá<sup>a</sup>, Ricardo M. Lima<sup>b,\*</sup>, Omar M. Knio<sup>b</sup>

<sup>a</sup>*Physical Science and Engineering Division, King Abdullah University of Science and Technology, Thuwal, 23955-6900, Saudi Arabia*

<sup>b</sup>*Computer, Electrical, and Mathematical Sciences and Engineering Division, King Abdullah University of Science and Technology, Thuwal, 23955-6900, Saudi Arabia*

---

## Abstract

Climate change mitigation requires strategic and timely investments. Renewable generation, carbon capture, and electric vehicles (EVs) are key mitigation technologies, yet their effectiveness depends on investment levels and mutual interactions. This study investigates the joint decarbonization of the power and transportation sectors, focusing on these technologies' competitive and cooperative effects. We develop a capacity expansion model that captures technology interactions while accounting for short-term variability in renewables and long-term climate change effects. The case study of Saudi Arabia by 2040 with a fixed emission target is examined. Although carbon capture reduces investment requirements, fuel subsidies significantly distort system costs. Still, system costs are 18% lower with carbon capture due to limited non-solar potential and high battery storage costs, which are significant barriers to achieving renewable penetration beyond 29%. A

---

\*Corresponding author.

Email addresses: [harif.fontechasanchez@kaust.edu.sa](mailto:harif.fontechasanchez@kaust.edu.sa) (Daniel Fontechá), [ricardo.lima@kaust.edu.sa](mailto:ricardo.lima@kaust.edu.sa) (Ricardo M. Lima), [omar.knio@kaust.edu.sa](mailto:omar.knio@kaust.edu.sa) (Omar M. Knio)

sensitivity analysis also reveals that storage costs must fall to a third of current projections to achieve higher renewable penetration. While EVs introduce additional demand, a 10% adoption rate yields substantial savings in the power sector, narrowing the cost gap between systems with and without carbon capture. Moreover, managed charging unlocks further synergies, allowing systems without carbon capture to even outperform those with it.

---

## 1. Introduction

The power and transportation sectors are the most significant contributors to global annual emissions, responsible for approximately 42% and 23%, respectively [1]. While there is widespread agreement on the urgency of decarbonizing these sectors, achieving emission targets cost-efficiently requires careful and strategic investment.

Decarbonizing the power sector hinges on the large-scale deployment of renewable energy. However, the spatiotemporal variability of renewables poses significant challenges. Firm generation must respond swiftly to balance supply and demand, but delays in its response necessitate costly measures such as energy storage and surplus reserves. These measures can substantially increase system costs as renewable penetration grows [2].

In parallel, the transportation sector is transforming, with electric vehicles (EVs) leading the charge. By 2022, 26 million EVs had been sold worldwide, solidifying their role as a pivotal solution for reducing carbon emissions from road transport, which accounted for approximately 16% of global emissions in 2021 [1, 3]. These vehicles offer several opportunities to enhance the decarbonization efficiency of both the power and transportation sectors, including [4, 5]:

1. Offsetting of tailpipe emissions: Emissions from conventional vehicles are avoided by using EVs instead. However, the abatement effect of EVs depends on the emissions involved in the electricity these demand.
2. Load-shifting: Through incentives to consumers, the demand from EVs is shifted throughout the day to periods with more and/or cleaner generation capacity available.
3. Vehicle to grid (V2G): EVs discharge electricity back to the grid during exceptionally high demand or low renewable generation periods. Hence, EVs with V2G partially substitute the role of battery energy storage (BES) units and/or generation units.
4. Reserves: Some firm generation and stationary storage units must remain idle to ensure reliability during contingencies. EVs with V2G capabilities enhance reliability by providing reserve services when connected but not charging or discharging, freeing firm generation capacity to meet the demand. [6].

Tailpipe emission offsetting is an inherent consequence of EVs, whereas load-shifting, V2G, and reserve services require additional incentives and infrastructure to manage the charging patterns of EVs. Despite the remarkable potential benefits of EVs, these also complicate the relationship between the power and transportation sectors. For instance, the abatement effect of EVs depends on the electricity mix used, and the demand from a large EV fleet can impact the electricity cost and emissions [5, 7, 8]. Therefore, it is crucial to assess to what extent the environmental benefits of EVs, load-shifting, and V2G justify the added complexity and required investments in infrastructure and incentives.

Carbon capture and storage (CCS) is another critical technology for re-

ducing emissions from fossil-based generation and the atmosphere. While direct air capture offers the potential for atmospheric emissions removal, its economic viability remains uncertain [9]. In contrast, CCS from flue gas—where carbon dioxide concentrations are over 250 times higher than in ambient air—offers significantly lower abatement costs [10]. The importance of this technology is underscored by its pivotal role in achieving the net-zero targets of countries like the US and China [11, 12]. Nonetheless, investment in point-source CCS competes with the large-scale deployment of renewables, highlighting the necessity of an integrated approach to decarbonization investment strategies.

Examining the interdependence of the power and transportation sectors, alongside carbon capture, is a complex challenge, even more so in the context of the imminent effects of climate change. For instance, the relationship between renewables and climate change effects is bidirectional. While renewables serve as a crucial instrument for mitigating climate change, their effectiveness may be compromised if the effect of climate change on renewable generation performance is not incorporated [13]. Besides, the electricity demand can change as the global temperature rises [14].

Global Circulation Models (hereafter climate models) are essential for understanding how future emission scenarios will influence the Earth’s climate system [15]. Climate models have consistently projected that climate change will increase solar irradiation variability, posing significant financial challenges for countries planning to rely heavily on solar power [13]. The availability of other renewable sources may either alleviate or exacerbate this issue, making it imperative to find cost-efficient pathways for achieving emission targets while considering the impending impacts of climate change.

Moreover, the vast dataset size of climate models is cumbersome for

optimization models with polynomial-time complexity. Similar data points can be clustered into representative datasets that capture spatiotemporal correlations and distribution characteristics of the original one. However, selecting an appropriate clustering algorithm is not straightforward. For instance, while k-means clustering is widely used, it often produces averaged values that overlook intra-period variance and underestimate extreme events, leading to underestimating the generation and storage capacities needed. [16–18].

Other significant complications arise from balancing renewable energy flows between batteries and navigating nodes with limited transmission capacity. A capacity expansion model can address this complex problem by determining the optimal mix of power system investments to minimize long-term costs while meeting demand and complying with technical and environmental constraints. These models consider investment options in generation, storage, and, where applicable, transmission while accounting for operational factors such as reserve requirements and emissions targets [19].

The following section reviews key studies on capacity expansion that explore the integration of electric vehicles (EVs), renewables, and/or carbon capture for climate change mitigation and adaptation, finally outlining the primary contributions of this work.

### *1.1. Literature overview and contribution*

Capacity expansion models have been extensively studied in the literature [19, 20]. However, many studies omit the variability of renewables in their formulations; most have ignored the combined effects of climate change on renewable generation performance and energy demand. Additionally, modeling simultaneously the power and transportation sectors, alongside carbon

capture, remains a globally underexplored area. Table 1 summarizes key reference studies on capacity investment for power systems, highlighting how renewable generation variability is included and whether climate change and the transportation sector are assessed.

Capacity expansion models are mainly continuous linear programs (LP). Continuous LP models are widely used because they simplify solving larger models, making them a common approach for generation and storage units. However, linear programs incorporating integer variables, known as MILP, are more frequently applied to transmission expansion problems.

The model size depends on the geographic area covered, the time horizon, and the employed spatiotemporal resolution (upper part of Table 1). Balancing these features is crucial to gaining insights into real-world dynamics within manageable computational times. For example, models from [22, 25, 26] adopt multi-year time horizons to analyze long-term investment trajectories. However, their coarse resolution overlooks the impact of renewable resource variability on the power system operation.

The time horizons of the model and that of the study do not always coincide. Table 1 differentiates both. For instance, Victoria et al. [24] studied 30 years of capacity expansion for Europe with a model’s time horizon of 6 years (1 year modeled for every 5 years). The authors apply this strategy to study long-term scenarios while preserving an hourly resolution for a model with 28 nodes.

Other models also aim to prioritize spatial resolution to attend to transmission line congestion and incorporate transmission expansion in the investment portfolio [2, 4]. Notably, Sioshansi and Denholm [4] employ this strategy to study the hypothetic role of Plug-in Hybrid Electric Vehicles (PHEVs) in the operation of the fuel-reliant ERCOT system of Texas in

Table 1: Summary of relevant literature and main contribution.

	Study						This work		
	[21]	[2]	[22]	[4]	[23]	[24]	[18]	[25]	[26]
Methodology Model Type	CEM LP	CEM MILP	CEM LP	UC MILP	CEM MILP	CEM LP	EFM LP	CEM MILP	CEM LP
Geographic Area Nodes	Europe 36	Saudi Arabia 34	World 15	Texas US 700	L.& F. Spain 6	Europe 28	Energy hubs Sweden 1	Colombia 5	Saudi Arabia 6
Time Period	2050	2040	2010-2100	2005	2050	2020-2050	2070-2090	2015-2030	2011-2030
Study's Time Horizon	1 year	1 year	90 years	1 day	1 year	30 years	20 years	15 years	19 years
Model's Time Horizon	1 year	1 day	90 years	1 day	1 day	6 years	1 year	1 year	19 years
Time Resolution	2 hours	1 hour	10 years	1 hour	1 hour	1 hour	1 hour	1 year	2 months
RE Data	H	H	H	-	H	Climate M.	Climate M.	H	Climate M.
RE Profiles Selection	Manual selection	-	-	ARIMA/ CDF-based	-	CDF-based	-	-	K-medoids Clustering
PV	✓	✓	✓	✓	✓	✓	✓	✓	✓
Wind Turbines	✓	✓	✓	✓	✓	✓	✓	✓	✓
CSP	✓	✓	✓	✓	✓	✓	✓	✓	✓
Storage	✓	✓	✓	✓	✓	✓	✓	✓	✓
GIS RE Inventory	✓								
Lifecycle Emissions									
Carbon Capture									
Transm. Expansion	✓	✓	✓	✓	✓	✓	✓	✓	✓
EV-load	✓	✓	✓	✓	✓	✓	✓	✓	✓
EV-V2G	✓	✓	✓	✓	✓	✓	✓	✓	✓

*CDF*: Cumulative Distribution Function, *CEM*: Capacity Expansion Model, *CSP*: Concentrated Solar Power,

*EFM*: Energy Flow Model, *GIS*: Geographical Information System, *H*: Historical, *L*, *E&F*: Lanzarote & Fuerteventura,

*LP*: Linear Program, *M*: Model, *MILP*: Mixed Integer Linear Program, *PV*: Photovoltaic Panels,

*RE*: Renewable Energy, *Transm.*: Transmission.

2005. The study reveals that PHEVs with V2G could have reduced operation costs by up to 0.5% with a vehicle adoption of 15%, which was enough to saturate the cost-reduction opportunity.

The impact of EVs in the grid can change in time and between locations, given the characteristic power matrix and the calculation approach employed [22, 24]. For instance, Carrión et al. [23] found that, by 2050, incentive-driven managed charging of EVs would reduce the total cost of an isolated power system in Spain by up to 3.85% and 2.7%, with and without V2G, respectively [23]. The capacity expansion model was formulated considering variability from demand, renewables, and EVs.

For short-term variability, Carrión et al. [23] used ARIMA statistical models parameterized separately for demand, solar radiation, and wind speed, together with heuristic scenario reduction techniques to achieve a tractable problem. However, the separate ARIMA models overlook potential correlations between solar radiation and wind speed. Despite this, the authors found a positive correlation between the optimal PV capacity and EV adoption, while no correlation is reported between wind power units and EVs. This result is consistent with other case studies [27, 28].

In a different approach, Perera et al. [18] used climate models to incorporate the effect of climate change on renewable generation. This method defined expected and extreme climate scenarios and applied in a hybrid stochastic-robust optimization framework. The authors highlight that ignoring the effect of low-probability scenarios and climate change on renewable generation can lead to overestimating the renewable generation potential and, therefore, to reduced reliability. This result is consequent with Souayfane et al. [17], who also prove that neglecting extreme weather data can lead to considerable performance gaps and a substantial underestimation of

the battery investment required to balance renewable generation variability.

Finally, incorporating an incomplete portfolio of alternatives can lead to biased solutions, regardless of the sophistication of the optimization model. For instance, Matar [26] demonstrated that including carbon capture in Saudi Arabia’s portfolio of alternatives has the potential to achieve its decarbonization goals at a lower cost than officially projected. Nevertheless, the study overlooks the impact of natural gas subsidies, the emissions and costs associated with transporting and storing captured emissions, and the emissions from constructing the carbon capture facility, which may lead to an overestimation of the abatement efficiency of on-flare carbon capture.

### *1.2. Main contribution*

The main contribution of this work is a systematic methodology for assessing decarbonization pathways for the power and road transportation sectors. To that end, both sectors are integrated into a deterministic generation and transmission expansion model subject to an annual emissions cap. The following highlights differentiate this work:

1. The optimization framework with hourly resolution captures the interactions among electricity demand, renewable generation technologies, fossil-based units, energy storage systems, transmission lines, carbon capture facilities, and electric vehicles (EVs) with and without managed charging.
2. A climate projection accounts for the effects of climate change on demand and renewable generation.
3. Spatial and temporal clustering techniques are employed to maintain computational tractability while preserving low-probability events and spatiotemporal correlations among renewable technologies [16–18].

4. Cost projections, technology efficiencies, and lifecycle emissions are included for all power sector technologies.
5. The analysis performed explores a range of emission targets, comprehensively evaluating the role of carbon capture and electric vehicles (with and without managed charging) in achieving a specific emission target.

### *1.3. Paper structure*

The structure of the paper is as follows: Section 2 presents the methodology employed, including the decision framework and problem statement for the capacity expansion model, the incorporation of parameters from climate data, and the inclusion of vehicle traffic patterns. Section 3 introduces the case study, and Section 4 presents and discusses the numerical results. Finally, Section 5 presents the conclusions of this work.

## **2. Methods**

The methodology consists of three subsections. Subsection 2.1 defines the decision framework. Subsection 2.2 describes how renewable generation profiles from climate models are incorporated. Lastly, Subsection 2.3 describes the methodology used to include traffic patterns for EVs.

### *2.1. Decision framework*

In this section, we describe the optimization problem used to analyze the role of EVs, carbon capture, and renewables in investment decisions based on the effects of emission constraints and climate-related variability.

### *2.1.1. Problem statement*

The optimization model is constructed from the power system operator's (SO) perspective. The aim is to determine investments and operations at their lowest cost in four key areas: (i) generation, (ii) storage, (iii) transmission, and (iv) carbon capture. For this, the capacity expansion model minimizes the the power system's annualized investment and operation cost under fixed annual emission limits. The tailpipe emissions avoided by incorporating EVs are offset in the emission balance.

A set of constraints defined by economic and technical parameters shapes the feasible region of the optimization problem. Economic parameters include investment, operation, and fuel costs, while technical parameters encompass energy efficiencies, ramping limits for firm generation, and the transmission capacities of both existing and candidate lines.

The portfolio of generation technologies includes photovoltaic panels (PV), wind turbines, concentrated solar power (CSP), combined cycle gas turbines (CCGT), and combined cycle gas turbines with point-source carbon capture (CCGT/CCS). CSP is modeled with three interconnected blocks: solar field collector (CSPF), thermal storage (CSPS), and power block (CSPG).

Figure 1 details all technology interactions in the optimization model.

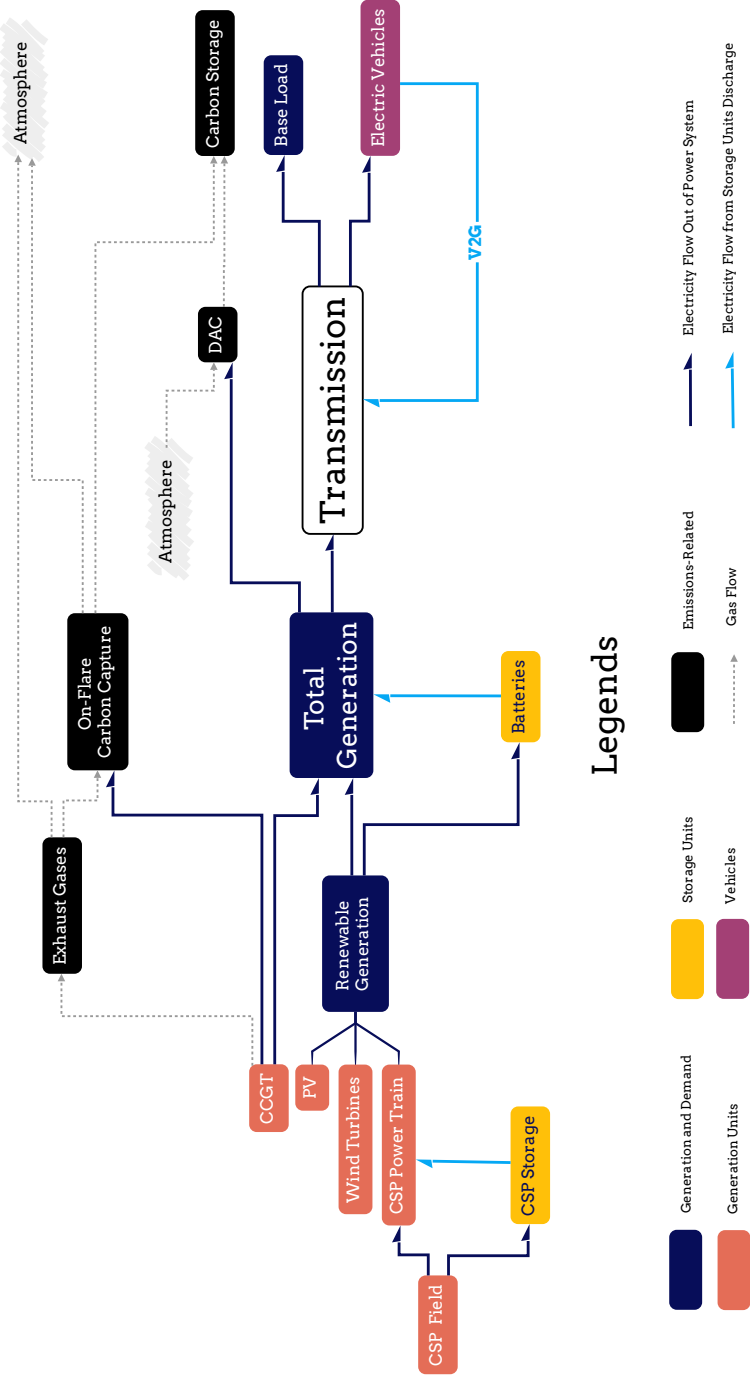


Figure 1: Flowchart of the main features included in the capacity expansion model. CCGT: Combined cycle gas turbines, CSP: Concentrated solar power, DAC: Direct air capture, V2G: Vehicle-to-grid technology.

Each node includes multiple renewable energy profiles, reflecting the spatial distribution of renewable generation potential within its area. In addition to renewable generation and point-source carbon capture (CCGT/CCS), the SO can achieve its decarbonization goals through investment in direct air capture (DAC). All captured emissions are assumed to be transported and stored in underground reservoirs.

The total electricity load originates separately from the base load and EVs. The aggregate charging demand of EVs is represented by a set of on-road discharging patterns and classified by the plug-in periods, i.e., the periods of the day EVs are expected to be connected to the grid. Two parameters finalize the definition of the EV demand: i) the size of the electrified vehicle fleet (which can optionally be set as a variable) and ii) the share of the fleet whose charging can be managed by the SO.

With managed charging, EV charging periods become decision variables within predefined connection windows, enabling load shifting. V2G functionality is also enabled with managed charging. The model guarantees that EVs are sufficiently charged after the connection periods while minimizing the total cost of the power system. Reserve balances are incorporated to ensure system reliability.

Figure 2 presents the workflow of the problem statement, for which the optimization model is the central feature. An epsilon-constraint analysis examines the correlations between renewable generation and EVs in the context of decarbonization goals. The analysis is performed with and without carbon capture to study its influence on each technology's role.

This study does not contemplate incentives for EV adoption or managed charging. Instead, the cost differences between epsilon-constraint scenarios define the upper limit of the budget for investment in EV infrastructure and

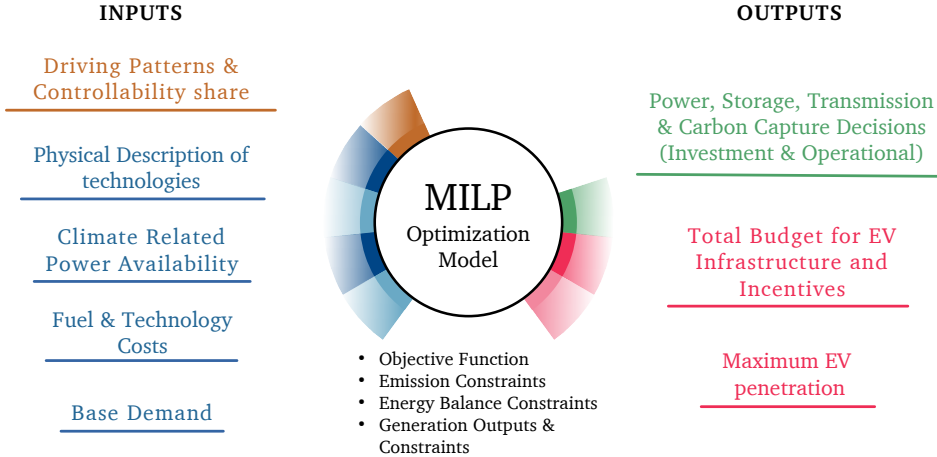


Figure 2: Workflow of the problem statement. MILP: Mixed integer linear program.

incentives throughout the strategy’s lifetime. The adoption of EVs is also evaluated as a variable to study the maximum EV adoption as a share of the total fleet that provides environmental benefits.

Finally, a greenfield approach is adopted for a one-year time horizon with an hourly resolution. The following subsection provides details on the mathematical formulation, whereas Section 2.2 describes how to incorporate climate-related data.

### 2.1.2. Mathematical formulation

The capacity expansion model is formulated as

$$\begin{aligned}
 \min_x \quad & c^\top x + d^\top y \\
 \text{st.} \quad & Ax \leq b \\
 & Wy \leq h - Tx \\
 & x \in X, X = \{x : x_j \in \{0, 1\} \forall x_j \in J, 0 \leq x_i \leq x_i^{ub}\} \\
 & y \in Y, \quad Y = \{0 \leq y \leq y^{ub}\}.
 \end{aligned} \tag{1}$$

The objective function is the annual cost, which incorporates annualized investment and operation costs. The investment variables  $x$  involve the decision on annualized capital investment, where binary variables determine investment in transmission lines and continuous variables define investment in generation, storage, and carbon capture. The operation variables  $y$  define the generation and load of each technology during operation.  $c^\top$  and  $d^\top$  are cost vectors, and matrices  $W$  and  $T$  and vector  $h$  define the feasibility region. These incorporate renewable generation and demand variability during the operation stage [29]. A detailed model formulation can be found in Note A of the Supplementary Information.

## *2.2. Climate-related renewable generation data and variability*

A climate model projection is used to generate renewable generation and demand data that is integrated into the optimization model. To ensure computational tractability in solving large-scale linear optimization problems, we apply spatial and temporal aggregation techniques based on clustering. Aggregation techniques inherently lose detail compared to the full-length dataset. This inherent error is more relevant for cases with time-binding constraints, such as those of storage units. In this study, we carefully select representative weeks to reach an acceptable balance between computational feasibility and model accuracy. The aggregation methodology—illustrated in Figure 3—is designed to reduce the dimensionality of climate and demand data while preserving variability, spatiotemporal correlations, and low-probability events. The following subsections detail this approach.

### *2.2.1. Attributes from climate models*

The initial dataset consists of three climate-related attributes: surface temperature data, wind speed, and shortwave surface solar irradiation (also

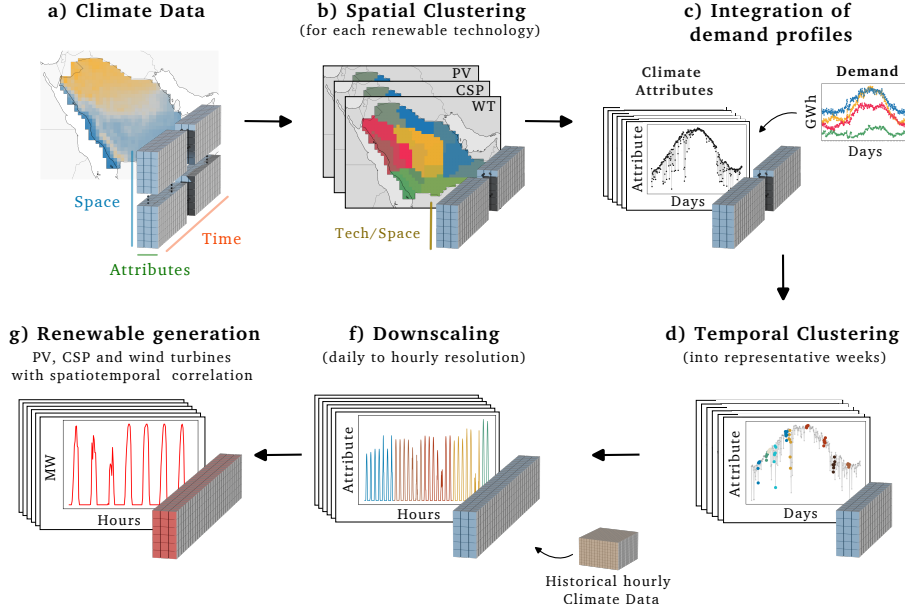


Figure 3: Clustering methodology to incorporate climate model attributes into renewable generation profiles.

known as global horizontal irradiation). In this work, the output variables from the climate model are referred to as “*attributes*” to differentiate them from the variables and parameters of the optimization model.

A dataset of attributes with daily resolution and spanning one year is employed as a starting point. A finer temporal resolution could capture intraday extremes but at the expense of a coarser spatial resolution. Moreover, climate models with daily resolution have been proven to effectively illustrate the potential effect of climate change on solar power output [13].

#### 2.2.2. Weighted spatial clustering

The area covered by the climate data is initially split into nodes. This step is relevant because transmission constraints are considered only between

nodes, not within them.

Then, each node and renewable technology is treated separately. The time series of all attributes are normalized, including a weighting factor to reflect their relative influence on the power output of a given technology. This approach ensures that the clustering process accounts for the varying impacts of different attributes on each renewable technology's performance.

For example, solar power output fluctuates by up to 8.1% with temperature in the range covered by the dataset (-5.4°C-41.1°C) [30]. Consequently, the weighting factor for temperature was approximated to 10%, given that, in comparison, solar radiation can cause a 100% variation in the power output of solar panels. Temperature plays a more significant and intricate role in the three blocks of Concentrated Solar Power (CSP), leading to a 100% weighting factor during normalization. The effect of wind speed on PV and CSP technologies is ignored, so a weighting factor of 0% was applied. Similarly, a 35% weighting factor was assigned to the temperature attribute for wind turbines, while the effect of solar radiation on wind turbines was considered negligible.

Subsequently, k-medoid clustering is applied to group areas with similar renewable generation potential (Figure 3b). The Python API of Scikit-learn is used for this purpose [31]. Each node and renewable generation technology is clustered independently. Within each node and technology, spatial clusters are represented by central points, or medoids, encompassing datasets of interrelated attribute time series spanning one year.

#### *2.2.3. Integration of demand profiles*

Elasticities are used to account for the effect of climate on demand profiles. Temperature and relative humidity from the selected climate model

are utilized to compute cooling and heating degree days (CDD and HDD) [32]. These metrics quantify the discomfort caused by extreme temperatures, with CDD associated with air-conditioning usage and HDD linked to heating-related electricity consumption.

CDD and HDD are calculated using the Steadman’s temperature-humidity index, which incorporates specific assumptions about heat exchange between humans and the environment [33].

The resulting climate-dependent demand profiles are integrated for each node in the attribute dataset (Figure 3c). This integration ensures that the seasonal correlations between demand and renewable generation are accounted for prior to temporal clustering.

#### *2.2.4. Temporal Clustering*

The k-medoid clustering algorithm is applied simultaneously to all attributes and spatial medoids to preserve spatiotemporal correlations (Figure 3d). Unlike k-means clustering, k-medoid clustering retains greater internal variability, as the chosen center corresponds to an actual sample from the original dataset rather than a smoothed average of attributes and time steps within a cluster.

The resulting temporal medoids are representative groups of seven consecutive days (representative weeks). Then, these are stacked into one single period of multiple weeks. Clustering consecutive days facilitates evaluating storage unit adaptability under variable but more realistic renewable generation conditions.

#### *2.2.5. Downscaling to hourly resolution*

Each day’s temporally correlated attributes—temperature, solar irradiation, wind speed, and electricity demand—are downscaled from daily to hourly

resolution using the analog statistical downscaling method [34]. A reference database comprising 20 years of historical data for the same month and node area coverage is utilized (Figure 3f). Monthly correspondence in the downscaling process is essential to preserve the seasonal characteristics of intraday generation profiles.

Hourly direct normal irradiance (DNI) from the selected historical days is incorporated to calculate the generation profiles of concentrating solar power (CSP) systems. The inclusion of DNI introduces no additional error, as its correlation with global horizontal irradiance (GHI) from the climate model remains constant for a given location and time of year. Both parameters are fixed for each step of the downscaling process, ensuring consistency in the generation profile calculations.

#### *2.2.6. Renewable generation profiles*

NREL's System Advisory Model (SAM) [35] and one year of historical climate data determine an optimized solar panel-inverter configuration [36]. Subsequently, the corresponding power output is calculated from the down-scaled renewable generation profiles. Similarly, NREL's SAM was used to calculate the power output of the CSP field collection block.

For wind turbines, the temperature-corrected power curve of a specific model is used to calculate the power generation profile. The wind speed attributes of climate models are extrapolated from the original 10 m height to the wind turbine hub height using the power law equation [37].

The profile weights from temporal clustering define the weight of each day during operation. Meanwhile, the weights from spatial clustering are combined with the total area of study to define maximum capacity constraints for renewable generation.

### *2.3. Traffic patterns*

The traffic patterns parameterize the energy consumption of vehicle aggregators based on typical traffic data. Each vehicle aggregator is characterized by periods when vehicles are connected to the grid (online periods) and periods when they are disconnected (offline periods). During offline periods, EVs are either in transit or areas without access to chargers.

Vehicles are assumed to move for a fraction of their offline periods. The energy consumption of vehicles is calculated based on their offline periods and, to a lesser extent, by the average speed limit of the road infrastructure. These patterns for offline energy consumption serve as input to the model, which ensures vehicles are sufficiently charged. The traffic patterns also serve as a basis for estimating the emissions offset by EVs. The charging strategy is optimized for EVs with managed charging, whereas EVs without this facility are charged as soon as they are connected to the grid.

## **3. Case Study**

The methodology is applied to Saudi Arabia, which is characterized by its oil-based economy and desert climate. For instance, more than 99% of the Saudi power capacity in 2022 was fossil-based and emitted approximately 260 million ton of carbon dioxide [38, 39]. In the Saudi Green Initiative, the government announced its goal to reach net zero emissions by 2060, which is expected to rely on its high solar power potential [39, 40]. However, the potential for other renewable sources to reconcile the disparities in the generation between day and night is limited [41]. Thus, conclusions drawn from the Saudi Arabian case can serve as a valuable reference for other nations with substantial solar power potential.

Furthermore, a state-owned company has recently announced the installation of 5000 public chargers for EVs in Saudi Arabia by 2030 [42]. However, literature on power system models with integrated EV load is almost nonexistent in Saudi Arabia. Only one study evaluated the effect of different charging patterns of EVs with a fleet share below 1% over a fixed power mix [5].

### *3.1. Input data*

The input data describing the Saudi system comprises four nodes (buses), three existing transmission lines, four candidate transmission lines, 72 candidate generation units, and eight candidate stationary storage units (four for BES and four for CSPS).

#### *3.1.1. Climate model*

The climate-related attributes are extracted and preprocessed from the CNRM-CERFACS-CNRM-CM6 global climate model from the CMIP-6 project [43]. More specifically, from the update experiment for the shared socio-economic pathway SSP245, which refers to a medium radiative forcing (or Representative Concentration Pathway - RCP 4.5) [44]. In line with this RCP scenario, the average temperature in the dataset in 2040 is 0.62°C higher than in 2020. The climate dataset has a 50 km x 50 km nominal spatial resolution and a daily temporal resolution. The curated dataset  $M$  is a 3x719x365 tensor composed of 3 attributes, 719 pixels, and 365 time periods.

#### *3.1.2. Demand Data*

The elasticities of residential demand to climate (represented by the CDD and HDD) for each region of the study case were published by Mikayilov [14]. The total demand was computed with a forecast for the industrial

sector [45]. More details on the forecasting procedure using econometric parameters and weather data, including the inherent assumptions involved, can be found elsewhere [46]. The total demand is 5.4% larger with the effect of climate change than without it. Note B of the Supplementary Information illustrates this effect.

### *3.1.3. Climate-related renewable generation*

*Clustering procedures.* The climate data was spatially reduced to 5 clusters per node and technology, for a total of 20 clusters per renewable technology, resulting in a tensor  $M'$  of size  $3 \times 60 \times 365$ . Afterward, the electricity demand is incorporated, and the time dimension of the dataset is reduced to 10 stacked representative weeks. The temporally clustered tensor  $M''$  is of size  $4 \times 60 \times 70$ .

The selection criteria for the number of representative weeks were i) a small within-cluster sum of squares (WCSS), ii) the existence of low probability weather conditions, and iii) tractability of the optimization problem. The WCSS quantifies the distance between each value in the dataset and its closest representative week. More details can be found in Note C of the Supplementary Information, including comparing attribute distributions before and after clustering.

*Downscaling.* 20 years of hourly historical data for the study area are extracted from NREL's National Solar Radiation Database [47]. For all days, the sum of absolute differences between datasets for all attributes was, on average, 0.05 and was below 2 in all cases. This means that differences in wind speed are at most 2 m/s only when there is a perfect match in average daily temperature and solar radiation. Figure 4 presents the summarized

climate profiles across all regions in the case study, highlighting the prevalence of high temperatures, high solar radiation, and low wind speeds. After appending the direct normal irradiation (DNI) from the historical data, the downscaled tensor has a size of 5x60x1680.

*Climate data to renewable generation.* The PV configuration and the CSP field block used in the SAM model were obtained using one year of historical data. Design parameters include the panel orientation throughout the year, the panel-inverter proportion for PV, and thermal dependence correlations.

The wind power output was calculated using the temperature-adjusted power curve of the Vestas V150/4200 wind turbine, previously installed in Dumat Al-Jandal, in the study region [48]. The wind speed was extrapolated to the turbine's hub height using a roughness length of 0.03 m, equivalent to minimal physical obstructions like trees and buildings, which is a reasonable assumption for most of the area covered in this study [37].

The average capacity factors for PV, CSP, and wind turbines in Saudi Arabia are 29%, 23%, and 21%, respectively. There are, in total, twenty candidates for each renewable technology (five per each of the four nodes) with profiles spanning 70 days. Each candidate technology is linked to a node, it has land-constrained maximum capacity, and preserves spatiotemporal correlation with other candidates and technologies in all nodes.

#### *3.1.4. Costs and technical parameters for the generation, storage, transmission, and carbon capture sectors*

All costs are calculated based on projections for 2040 using a moderate technology development scenario, which is the middle point between those proposed by the technology baseline developed by NREL [49]. All costs are given in 2024 dollars, and the capital costs are annualized with a discount

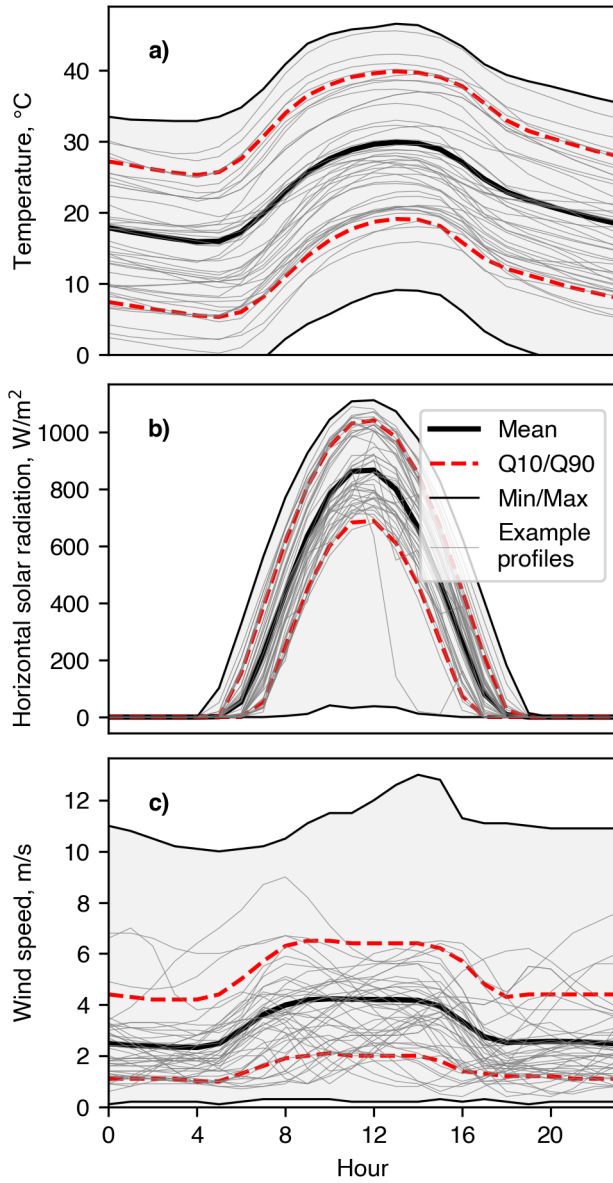


Figure 4: Statistical summary of a) temperature, b) horizontal solar radiation, and c) wind speed for all regions of the case study. The percentiles and maximum/minimum bounds are calculated hourly for all instances. Example profiles are illustrated for reference.

rate of 7%. The main techno-economic parameters for generation are given in Table 2. The costs of CSP are given separately for each of the three interconnected blocks: solar field collector (CSPF), thermal storage (CSPS), and power block (CSPG). Other parameters include a maximum capacity factor of 90% for CCGT units to account for capacity fading throughout the lifetime of the units. Also, reserves are set to cover at least 3% of the demand.

The emission rate of all generation units incorporates emissions throughout their lifecycle. For instance, the emission rate of CCGT of 468.5 kg CO<sub>2</sub>/MWh incorporates point-source emissions and upstream emissions from natural gas production and plant construction [50, 51]. Still, the upstream emissions from natural gas production of 9.6 kg CO<sub>2</sub>/MWh have a negligible share compared to those from plant construction (14.25%) and point-source emissions (85.75%) [52].

Carbon capture and storage (CCS) in CCGT includes an energy penalty of 11% for an emission capture efficiency of 95%, reflected in the heat rate of the generation units [49]. Carbon dioxide transport and underground storage are incorporated with costs of \$5.2 and \$8.0 per ton of CO<sub>2</sub>, respectively, corresponding to a middle cost for a 3.2 Mtpa CO<sub>2</sub> capacity and a transportation distance of 100 miles [53]. This extra carbon dioxide handling and storage cost is reflected as an additional \$0.8/MWh in the non-fuel variable O&M costs of CCGT with CCS.

The domestic price of natural gas is set at \$1.25/mmBTU [26], which reflects i) the low cost of natural gas extraction in Saudi Arabia and ii) the aggressive domestic subsidies to fuel. For instance, the average price of natural gas for electric power in the US in the last 20 years has been four times larger, at \$5.2/mmBTU [54]. The effect of the natural gas subsidy is

further discussed in Sections 4.4 and 4.10.

Table 2: Technoeconomic parameter projection of generation by 2040, in 2024 USD.

Parameter	CCGT	CCGT/CCS	Wind	PV	CSPF	CSPG
Capital Cost (\$/kW)	1475 <sup>1</sup>	2452 <sup>1</sup>	1439 <sup>1</sup>	941 <sup>1</sup>	3288 <sup>1,2</sup>	1740 <sup>1,2</sup>
Lifetime (years)	35 <sup>3</sup>	35 <sup>4</sup>	20 <sup>1</sup>	25 <sup>1</sup>	25 <sup>1,2</sup>	25 <sup>1,2</sup>
Fixed O&M cost (\$/kW-y)	32.8 <sup>1</sup>	54.5 <sup>1</sup>	31.1 <sup>1</sup>	16.1 <sup>1</sup>	46.5 <sup>1,2</sup>	24.6 <sup>1,2</sup>
Var. O&M cost <sup>†</sup> (\$/MWh)	2.17 <sup>1</sup>	4.48 <sup>1</sup>	6.73 <sup>1</sup>	0.0 <sup>1</sup>	0.0 <sup>1,2</sup>	0.0 <sup>1,2</sup>
Heat rate (GJ/MWh)	6.1 <sup>1</sup>	6.7 <sup>1</sup>	-	-	-	-
CO <sub>2</sub> emissions (kg/MWh)	468.5 <sup>5,6,7</sup>	146.5 <sup>3,5,6,7</sup>	46.9 <sup>8</sup>	28.9 <sup>9</sup>	-	40.0 <sup>10</sup>
Ramping limits	30% <sup>11</sup>	50% <sup>11</sup>	-	-	-	-

<sup>†</sup> Variable O&M costs exclude fuel costs for CCGT generation.

<sup>1</sup> [49], <sup>2</sup> [55], <sup>3</sup> [26], <sup>4</sup> [56], <sup>5</sup> [51], <sup>6</sup> [50], <sup>7</sup> [52], <sup>8</sup> [57], <sup>9</sup> [58], <sup>10</sup> [59], <sup>11</sup> [60].

Direct air capture is incorporated with a cost of \$250/ton of CO<sub>2</sub>, which is a middle point in the wide range of estimated costs of \$94 - \$1000/ton of CO<sub>2</sub> [9]. The electricity demand from DAC is set at 614 kWh/ton of CO<sub>2</sub> under the assumption of waste heat availability [61]. The emissions associated with adsorbent utilization and plant construction are 4.5% and 1.5% of the emissions captured [62]. Table 3 describes the parameters for stationary storage. BES and CSPS differ significantly in their lifetime and energy-to-power ratios, which determine the annualized cost per cycling power. The initial and final storage capacity is assumed. In contrast, the limits in the maximum and minimum SoC aim to incorporate a mild decay in the capacity of BES throughout their lifetime.

The transmission network and node definition follow the nomenclature used until 2020 by the Water and Electricity Regulation Authority of Saudi

Table 3: Technoeconomic parameters projection of stationary storage by 2040, in 2024 USD.

Parameter	BES [49]	CSPS [49, 55, 63]
Capital Cost (\$/kWh)	355	480
Lifetime (years)	10	25
Hours of capacity to power (MWh/MW)	4	15
Charging efficiency (MW/MW)	92%	95%
Discharging efficiency (MW/MW)	92%	91%
Initial/final SoC	70%	70%
Maximum SoC	95%	100%
Minimum SoC	5%	0%

Arabia [64]. The four nodes are named East, Central, West, and South, interconnected by three transmission lines. Table 4 details the existing and potentially added transmission capacity. Five candidate lines are considered for transmission expansion, with an annualized cost of \$24,000/km [2, 65]. More details on the topography of the transmission system of Saudi Arabia can be found elsewhere [2, 65].

### 3.1.5. Vehicle parameters

Five vehicle groups per node are defined based on traffic count data. Note D of the Supplementary Information provides their definition and fit with the reference traffic data.

Each vehicle is assumed to spend 15% of its offline time in motion, equating to between 6.9% and 12.5% of the total time. These times are a conservative approach. For instance, the traffic database employed reports 1.77 million cars sensed daily and a total fleet of 15 million passenger vehicles

Table 4: Technoeconomic parameters of existing and candidate transmission lines.

Line	Node from (pu)	Node to (pu)	Lenght (km)	Existing capacity (MW)	Potential added capacity (MW)
1	East	Central	400	5500	2500
2	East	South	1150	0	2200
3	Central	West	850	2200	1000
4	Central	South	800	0	2000
5	West	South	470	2000	2000

[5, 66]. Assuming each vehicle is sensed only twice (roundtrip), the average utilization rate is 5.75%. Moreover, a travel survey in Saudi Arabia indicates that the average daily mileage is below 40 km, and vehicles are used for less than 30 minutes daily (around 2% of the total time) [67]. Furthermore, these assumptions align with conclusions from other driving surveys [67–69].

The total vehicle fleet is extrapolated to 21 million units and distributed across nodes in proportion to the projected population growth and current population distribution. Additional parameters for EVs can also be found in Note D of the Supplementary Information.

### 3.2. Model Implementation

The model is built in GAMS, and all simulations are performed with CPLEX version 14.2.0. A parallelized compute node resolution strategy is followed using a High-Performance Computing (HPC) cluster. All nodes have processor speeds between 2.0 and 4.2 GHz and 6 GB of allocated RAM. The linear model comprises 638,554 constraints, 2,623,435 million continuous variables,

and five binary variables. All optimization runs achieved global optimality in less than 48 hours, with an average runtime of approximately 9 hours.

## 4. Results

Reference results are first presented for two cases: i) a fully renewable system and ii) a base case aligned with a 2040 emissions target. Then, a detailed analysis is presented for the base case to exemplify the methodology and highlight the findings' significance.

We begin by assessing the economic impacts of carbon capture and uncontrolled EVs (i.e., without managed charging) relative to the base case. Next, we evaluate their combined effects. We then introduce the multiple features of managed EV charging, analyzing its impact on the system configuration and operation.

Afterward, we present the bounds on the EVs' abatement potential and a sensitivity analysis of battery energy storage (BES) costs. Lastly, we discuss the limitations and policy-relevant opportunities arising from these findings.

### 4.1. Fully renewable case

Figure 5a contrasts the annual cost of a power system for multiple annual emission targets. These costs include both annualized investment and yearly operational expenses. The black circle in Figure 5a illustrates the case for a fully renewable system. It emits around 19 million ton of CO<sub>2</sub> from the construction of facilities. This system has an annual cost of 96 billion USD (2024), equivalent to 9% of the Saudi GDP in 2024. This case includes 347 GW of renewable generation capacity and 4,800 GWh of BES, with 67% of the generation capacity coming from PV and the remainder from wind.

Notably, CSP did not appear as part of a cost-competitive generation mix in this or any of the other cases evaluated.

#### *4.2. Base case: 2040 emission target*

The base case is defined by an annual emissions target of 100 million ton of carbon dioxide for the power sector, consistent with 2040 projections under an announced policy scenario [26]. The corresponding annual cost—represented by the white circle in Figure 5a—is estimated at \$44 billion USD. This system comprises 267 GW of generation capacity and 1,035 GWh of BES, with the generation mix consisting of 27% CCGT, 43% PV, and 30% wind. Renewable sources provide 68% of the total electricity supply. In the following subsections, we elaborate on alternatives to reduce the annual cost required to meet the same emissions target.

#### *4.3. Economic impact of EVs*

Adopting EVs generally reduces the annual costs required to meet emission targets. Fuchsia lines in Figure 5 reflect the lower costs of systems with uncontrolled EVs, driven mainly by their abatement effect of offsetting tailpipe emissions. For instance, a 10% EV adoption reduces by 24% the annual cost required in the power sector to achieve an emission goal of 100 million ton of carbon dioxide (from white to fuchsia circle Figure 5a). Alternatively, a 10% EV adoption can cut annual emissions from 100 to 68 million ton of carbon dioxide for a fixed power sector budget of \$44 billion (as shown by the shift from the white point to the fuchsia square in Figure 4b). In all cases, the potential benefits of EVs grow as annual emission limits are lowered.

For the base case, these savings translate to \$4,900 per EV (Figure 5c). This value sets an upper limit on the budget for charging infrastructure and

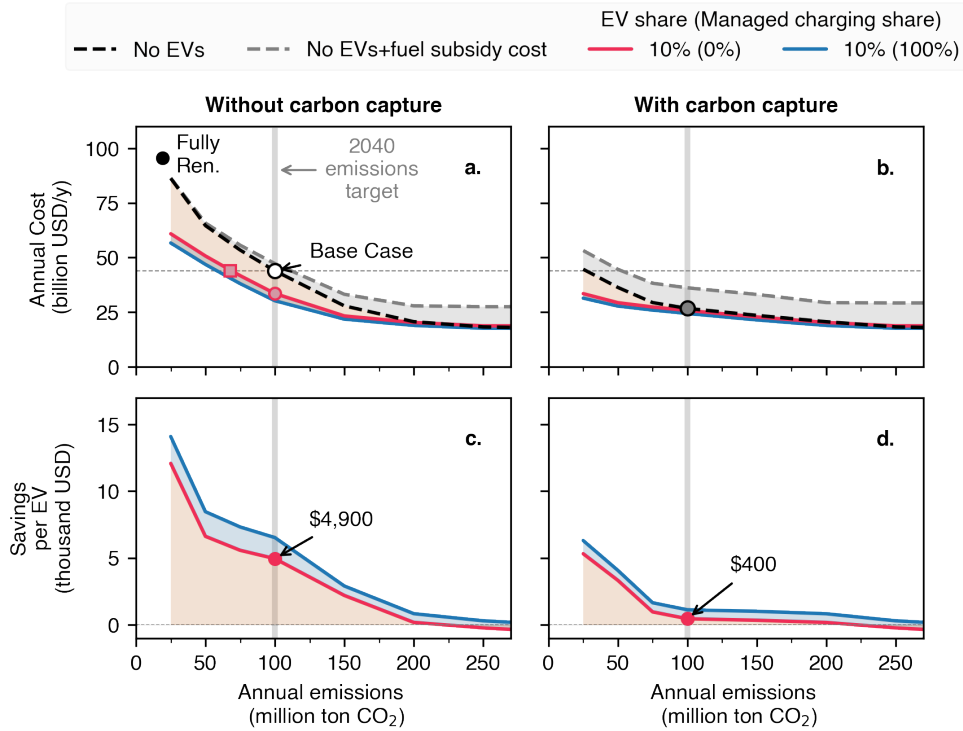


Figure 5: Effect of EVs and carbon capture on annual costs to meet decarbonization targets. Pareto fronts for: a) systems without carbon capture, and b) systems with carbon capture. The dashed black lines represent cases without EVs. Colored lines correspond to a 10% EV adoption share relative to the projected 2040 passenger vehicle fleet, with managed charging levels of 0% (pink) and 100% (blue). Shadow costs from fuel subsidies are included as gray dashed lines. Panels c) and d) show savings per EV for systems without and with carbon capture, respectively. These values indicate the maximum allocable budget for EV infrastructure and incentive programs. Red areas highlight cost reductions achieved through uncontrolled EV adoption, while blue areas reflect additional savings from managed charging. The estimated 2040 emission goal for Saudi Arabia is a middle point between the announced goals by 2030 and the Net-Zero emissions goal of 2060 [26].

incentives. Results for a 1% EV adoption share are also presented in Note E of the Supplementary Information, where savings of \$5,400 per EV are achieved for the same base case. In other words, the economic benefits for

every additional 1% of EV adoption drop on average by \$55. After factoring in charging infrastructure costs, incentive policies for buyers can be adjusted to account for the slight reduction in benefits as EV adoption grows.

Only in specific scenarios do EVs prove to be an ineffective abatement alternative. This scenario is most visible in Figures 5c and 5d, where a 10% EV adoption coupled with annual emissions exceeding 250 million ton of CO<sub>2</sub> results in economic loss. In such cases, the 6% increase in total load and the minimal abatement effect of EVs charging from a fossil-based grid do not justify the additional generation costs.

However, as little as 6% renewable capacity share is enough to enhance the EVs' abatement potential, favoring the inclusion of the first 1% EV share with net emission reductions. Alternatively, managed charging can turn EVs into an effective decarbonization solution, even when powered entirely by gas-based electricity. The consistent savings from EVs with managed charging are evident in the blue line of Figure 5c, which incorporates the managed charging effect and remains positive in all conditions. These findings demonstrate the critical role of complementary strategies in maximizing the environmental benefits of EVs.

#### *4.4. Economic impact of carbon capture*

With carbon capture as part of the portfolio of alternatives, annual costs drop by 39% compared to the base case, reaching 27 billion USD (gray circle in 5b). Two key factors influence the economic viability of carbon capture in Saudi Arabia: i) large domestic fuel subsidies and ii) the limited renewable potential for balancing solar power.

From the power generator's perspective, substantial subsidies to natural gas are a convenient cost-reduction factor. However, from a national

perspective, fuel subsidies distort the actual cost of power system configurations. The shadow cost of fuel subsidies was calculated for the solutions obtained from the optimization model. These were computed based on the fuel consumption and the price gap between the domestic gas price (\$1.25/mmBTU) and the average Henry Hub natural gas spot price in the last 20 years (\$5.2/mmBTU) [70]. The gray dashed lines in Figures 5a and 5b reflect the magnitude of this hidden cost. Although incorporating fuel subsidy costs increases the annual costs of a case with carbon capture by 35% (Figure 5c), the annual cost remains 18% below that of a case without carbon capture.

Secondly, minimal wind power capacity is available to balance solar generation. In that context—and in the absence of cost-effective alternatives like hydropower (excluded from this model)—BES emerges as the primary solution for managing solar power fluctuations despite its high capital costs.

The abatement potential of point-source carbon capture becomes saturated near the target of 100 million ton of carbon dioxide. Beyond this point, further emissions reductions lead to sharp cost increases driven by substantial investments in renewables, BES, and DAC. This and other inflection points are most visible in the marginal abatement costs presented in Note F of the Supplementary Information.

#### *4.5. Effect of uncontrolled EVs and carbon capture on the power system configuration*

The CCGT-dominated configurations in cases with carbon capture benefit less from EV integration, with savings for the base case reaching around \$400 per uncontrolled EV (Figure 5d). However, EV-related savings can become up to six times greater under more ambitious emissions goals when

effective abatement through carbon capture starts to saturate.

Figure 6 presents the installed generation capacity for multiple cases, each differentiated by i) annual emissions limit, ii) share of EVs, iii) share of EVs with managed charging, and iv) the presence or absence of carbon capture.

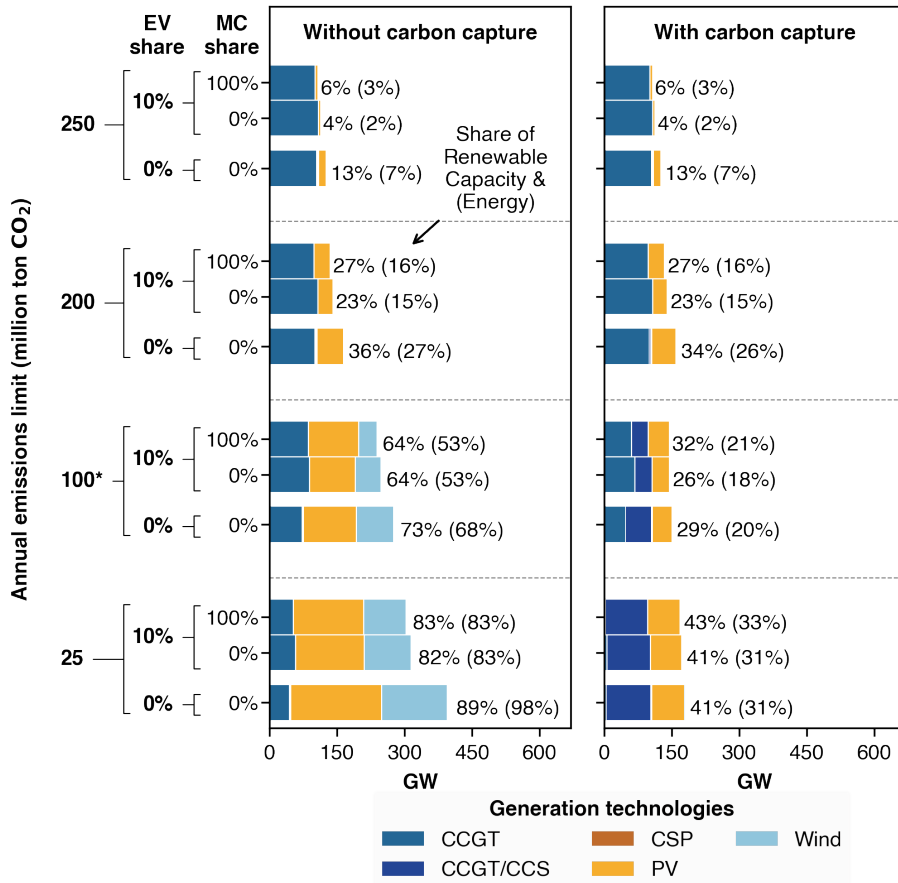


Figure 6: Installed capacity dependence with i) annual emission limit, ii) share of EVs, iii) share of EVs with managed charging (MC), and iv) the presence or not of carbon capture. The renewable capacity share and energy shares (in parentheses) are indicated for each case. The base case is for an annual emission target of 100 million ton CO<sub>2</sub>.

The most evident contrast in Figure 6 is the total capacity between systems with and without carbon capture. The difference between configurations reflects the higher utilization factors of CCGT units compared to renewables and, more importantly, the shift in emission abatement strategy—from relying on renewables to using CCGT with CCS. Moreover, wind power is not installed in conjunction with carbon capture. For instance, renewable generation is below 29% of the total installed capacity for the base case emission target of 100 million ton of carbon dioxide.

The high cost of BES in a system without carbon capture also forces regional interdependence as an alternative to balance renewable fluctuations. Consequently, more transmission capacity is incorporated, growing with ambitious emissions targets. In contrast, a system with carbon capture does not profit from building additional transmission capacity. Note G of the Supplementary Information provides more details on transmission expansion and exemplifies transmission flows between nodes.

Notably, although EVs add load to the power system, their integration reduces the total capacity and costs required to meet emission targets. In such scenarios, more CCGT (without carbon capture) replaces renewable generation and CCGT/CCS, with EVs offsetting emissions.

Table 5 details cost and configuration changes due to EVs for the base case (without carbon capture). A 10% EV adoption yields a 24% reduction in annual costs. Investment in solar and wind power declines by 12% and 30%, respectively, while investment in CCGT capacity compensates for these drops, rising by 24%. In addition to shifts in generation technologies, BES investment drops by 67% and amply dominates the savings.

Additionally, Table 6 presents the effect of EVs for the base case in the presence of carbon capture. In this case, the cost driver is the displacement

of PV and, to a greater extent, CCGT/CCS by CCGT. A higher utilization factor is also achieved in the installed CCGT units with and without carbon capture. As a result, the combined energy output from CCGT units grows by 9%, more than the 5% growth in total installed capacity, while annual costs decline by 4%. These findings highlight how EVs can reshape power system configurations while also being influenced by them.

#### *4.6. Managed charging: Synergies between EVs and the power sector*

In this case, EVs adjust their charging and discharging profiles in response to the power sector's needs without affecting driving patterns. The primary advantage of EVs lies in their ability to reduce the environmental impact of the vehicles by eliminating tailpipe emissions. However, the integration of the power and transportation sectors reveals additional improvements. EVs with managed charging facilitate bidirectional communication between sectors, which results in significant cost reductions (blue lines in Figure 5). In particular, managed charging substitutes for BES, enabling more efficient investment in solar panels.

In a case without carbon capture, annual costs decrease by seven additional percentage points when managed charging is implemented (Table 5), equivalent to additional savings of \$1,600 per EV. Interestingly, investment in wind turbines drops with managed charging, with PV substituting for their green energy contribution.

In a system dominated by carbon capture, EVs with managed charging fully substitute BES, reducing annual costs by five additional percentage points (Table 6). These savings more than double the effect of uncontrolled EVs, resulting in further savings of \$680 per EV.

Table 5: Effect of EVs and managed charging in a case without carbon capture.

	Base Case	+EVs Uncontrolled	+EVs Managed charging
Emissions limit ( $10^6$ t CO <sub>2</sub> /y)	100	100	100
EV-adoption share	0%	10%	10%
EVs with managed-charging	0%	0%	100%
Annual Cost (bn USD/y)	44	34 (-24%) <sup>1</sup>	30 (-31%)
Annual+Shadow Cost(bn USD/y) <sup>2</sup>	47	38 (-18%)	<b>33.6</b> (-29%)
Savings in BES/Net savings	-	84%	75%
<b>Technology break-down:</b>			
PV (GW)	115	102(-12%)	112 (-3%)
Wind (GW)	81	57 (-30%)	41 (-49%)
CSP (GW)	0	0 (-)	0 (-)
CCGT (GW)	71	88 (+24%)	86 (+21%)
Energy CCGT (TWh)	178	270(+51%)	270(+52%)
BES (GWh)	1035	345 (-67%)	217 (-79%)
<b>Share of managed-charging savings from:</b>			
Load shifting only	-	-	53%
Load shifting + V2G <sup>3</sup>	-	-	~100%

BES: Battery energy storage, CSP: Concentrated solar power, CCGT: Combined cycle gas turbines.

<sup>1</sup> Values in parenthesis denote variation from the base case.

<sup>2</sup> Includes shadow costs from fuel subsidies.

<sup>3</sup> Excluding reserves.

#### 4.7. EVs to close the cost gap between configuration alternatives

The above results consistently show that EV integration and managed charging cost reductions are more pronounced in systems without carbon capture.

Table 6: Effect of EVs and managed charging in a case with carbon capture.

	Base Case +CCS	+EVs Uncontrolled	+EVs Managed charging
Emissions limit ( $10^6$ t CO <sub>2</sub> /y)	100	100	100
EV-adoption share	0%	10%	10%
EVs with managed-charging	0%	0%	100%
Annual Cost (bn USD/y)	26.7	25.8 (-4%) <sup>1</sup>	24.4 (-9%)
Annual+Shadow Cost (bn USD/y) <sup>2</sup>	36.1	36.0	<b>34.2</b> (-5%)
		(-0.3%)	
Savings in BES/Net savings	-	-1%	6%
<b>Technology break-down:</b>			
PV (GW)	42	38 (-8%)	46 (+11%)
Wind (GW)	0	0 (0%)	0 (0%)
CSP (GW)	0	0 (0%)	0 (0%)
CCGT (GW)	47	68 (+45%)	62 (+31%)
CCGT/CCS (GW)	55	39 (-29%)	37 (-33%)
CCGT+CCGT/CCS (GW)	102	107 (+5%)	99 (-3%)
CCGT+CCGT/CCS Energy (TWh)	435	473 (+9%)	461 (+6%)
BES (GWh)	12	13(+7%)	0.0 (-100%)
<b>Share of managed-charging savings from:</b>			
Load shifting only	-	-	46%
Load shifting + V2G <sup>3</sup>	-	-	93%

CCS: Carbon capture and storage, BES: Battery energy storage, CSP: Concentrated solar power, CCGT: Combined cycle gas turbines.

<sup>1</sup> Values in parenthesis denote variation from the base case.

<sup>2</sup> Includes shadow costs from fuel subsidies.

<sup>3</sup> Excluding reserves.

Conversely, the shadow costs from fuel subsidies exert a greater influence

on systems with carbon capture. When all factors are considered, a notable finding emerges: systems without carbon capture can perform comparably to, and in some cases even outperform, those with it. This result is a noteworthy driver for redirecting current natural gas subsidies toward electrification programs. For instance, under managed charging scenarios (embolden values in Tables 5 and 6), the system without carbon capture is more economical. It is also important to note that while this analysis does not account for investments in charging infrastructure or incentives, these are the same for both cases, considering a fixed EV share and controllability condition.

#### *4.8. A closer look at managed charging: load shifting, V2G, and reserves*

In this section, we detail the multiple effects of managed charging. The load balance in Figures 7a and 7b shows the interplay of generation units, BES, and EVs for a 10% EV adoption with managed charging.

The importance of BES for intraday balancing of solar power stands out in a system without carbon capture, while this phenomenon does not occur in a system with carbon capture. Figures 7c and 7d are a zoomed-in representation of the same balances of Figures 7a and 7b, respectively. These illustrate load shifting in EVs, whose charging patterns (negative axis) adjust to periods when energy is most available and/or when grid emissions are lower. V2G is also visible (positive axis) as an alternative to balance fluctuations in renewable generation. For cases with carbon capture, V2G mostly occurs in the late afternoons, facilitating the transition from a solar-dominated configuration during the day to a CCGT-dominated one at night.

As presented at the bottom of Tables 5 and 6, load shifting and V2G contribute almost equally to the managed charging benefits. These results

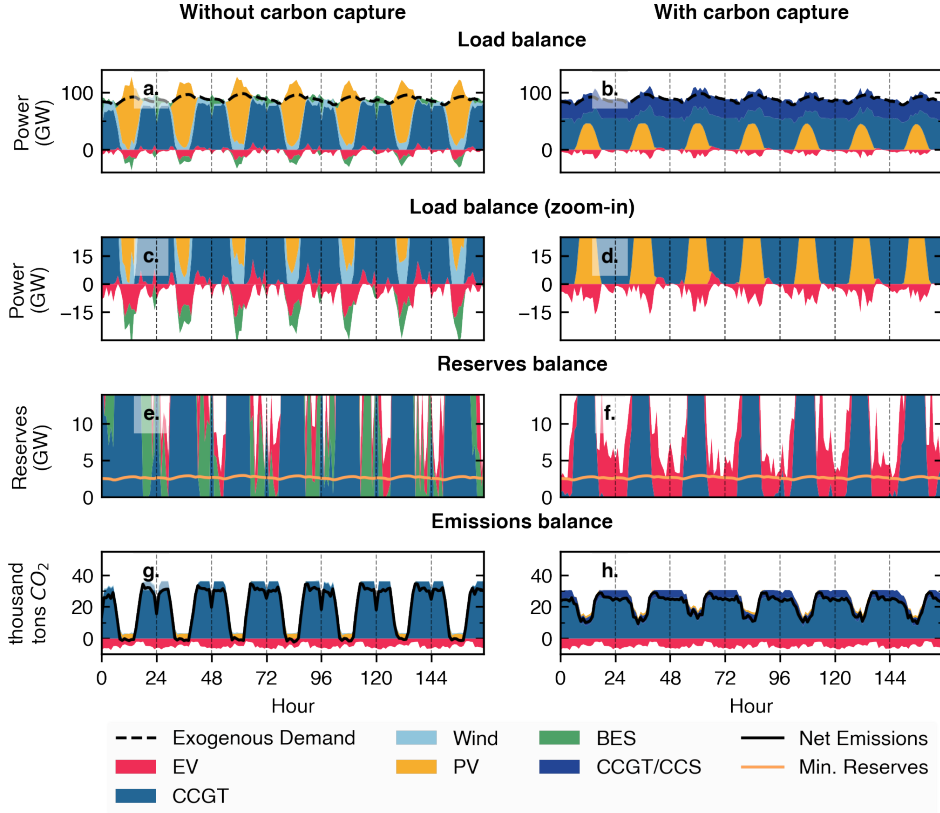


Figure 7: Load balance, reserve balance, and emission profiles for cases without (left) and with carbon capture (right). Plots are for days 49 to 55, which can be traced back to a week in September in the original climate dataset. The cases consider a 10% EV adoption share, 100% share of EVs with managed share, and an annual emission target of 100 million ton of carbon dioxide.

provide a benchmark for assessing whether the additional investment in bidirectional charging infrastructure for V2G justifies its cost. Moreover, the savings breakdown can guide the allocation of budgets for load-shifting and V2G incentive programs.

The third benefit of managed charging in EVs is reserve services. These are used sporadically in a case without carbon capture, as BES generally

meet reserve requirements during periods of high CCGT utilization. This case is illustrated in Figure 7e, where the available and the minimum reserves needs are contrasted. Meanwhile, with carbon capture, EVs provide reserve services more frequently, displaying a strong seasonal trend: they are utilized predominantly during summer when the load is highest (Figure 7f). In this case, reserves from EVs help reduce the total CCGT capacity needed, as more firm capacity can be effectively used when it is needed most. Consequently, reserve services represent 7% of the economic benefit of managed charging for a case with carbon capture (Table 6).

It is important to note that although reserve services have a small effect compared to V2G and load shifting, they can be profited from without significant extra costs or potential EV battery degradation. Figure Note H in the Supplementary Information exemplifies typical EV battery profiles, highlighting periods of charging, V2G, and reserve service contributions.

Finally, figures 7g and 7h illustrate the emission fluctuations from the power sector and those offset from EVs. For instance, 19% of the power sector emissions are offset by the tailpipe emissions avoided through EV adoption. This emission abatement effect does not saturate below 10% EV adoption—meaning that, within this range, more EV adoption consistently leads to lower overall emissions. This conclusion highlights a strong case for investing in EV infrastructure and supportive policy incentives. The following subsection examines the extent to which EVs can serve as an effective decarbonization strategy.

#### *4.9. There is plenty of room for EVs*

Figure 8 illustrates the EV shares beyond which net emissions cannot be further reduced. In these cases, the emissions offset by EVs and those from

the additional load required by EVs cancel out. Therefore, further EV adoption increases emissions and/or power system costs.

A remarkable finding is that minimal efforts in the grid are needed to unlock mass adoption of EVs as a competitive emission abatement alternative. For instance, a system with as little as 6% renewable capacity and equivalent emissions of 250 million ton of CO<sub>2</sub> per year already benefits from an EV adoption as high as 4%. To put this EV share value into perspective, it is comparable to the EV share of 3.6% achieved by the European Union in 2023 after years of incentivizing policies [71]. Not surprisingly, the EVs' decarbonization competitiveness increases as electricity emissions decline.

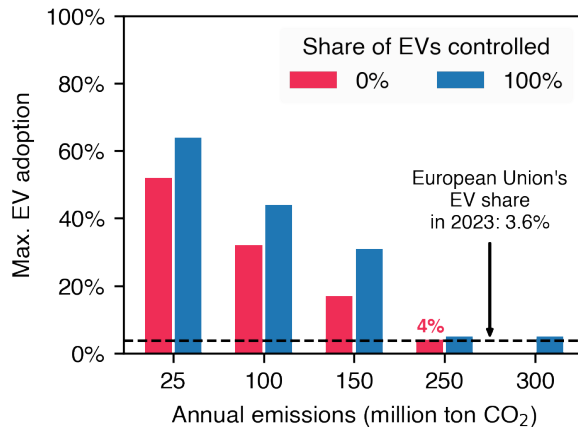


Figure 8: Maximum share of EVs that results in a competitive decarbonization alternative for a case without carbon capture. EV adoption beyond these values results in either higher costs or increased emissions due to the additional load required.

Managed charging increases the abatement potential of EVs, mainly when the power system emits less CO<sub>2</sub> and the synergies with the growing renewable share become more evident. However, these EV share limits neglect infrastructure and incentive costs for EVs. Hence, a feasible and

cost-efficient EV adoption should be smaller.

#### *4.10. Effect of battery energy storage costs*

A sensitivity analysis on BES costs was conducted to understand how cost reductions beyond projected levels might further impact the role of renewables and carbon capture.

Figure 9a presents the power system costs for the base case emissions target, with and without carbon capture. For simplicity, EVs were excluded from this analysis. The cost of a system without carbon capture gradually falls with BES costs (yellow lines), unlike with carbon capture (blue lines). After shadow costs from fuel subsidies are incorporated (solid lines), systems with and without carbon capture reach equivalent costs when the BES costs fall to 36% of the projected values. Only then does renewable capacity share increase beyond 29% in cases with carbon capture (Figure 9b). Additional cost reductions in BES potentially increase the renewable share to up to 72%.

Although these cost reductions are ambitious, improvements in BES technology have already exceeded expectations. For example, since lithium-ion batteries were first commercialized in 1991, their cost per megawatt-hour has decreased by about 97%, consistently exceeding previous estimates [72].

#### *4.11. Limitations and opportunities*

This study does not explicitly include the investment costs of an EV charging infrastructure or incentive programs. Instead, it quantifies the potential economic incentives from a national systems perspective. For reference, the combined cost of residential and non-residential chargers for 2.6 million EVs in the US was estimated at approximately \$2.2 billion for 2019–2025,

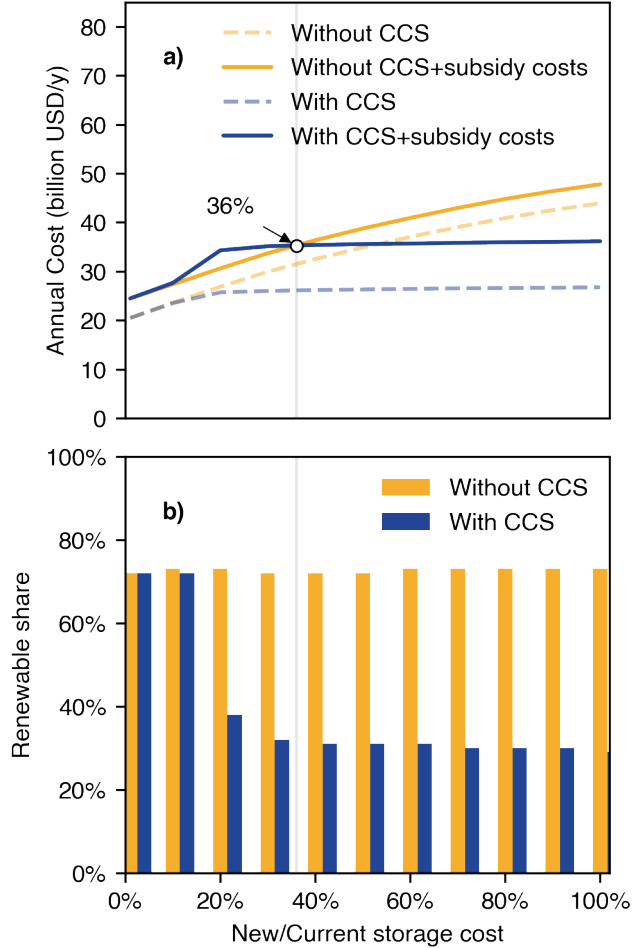


Figure 9: Sensitivity analysis of energy storage cost over a) the annual power system costs and b) the renewable share. Study case with a 100 million ton of CO<sub>2</sub> target and without EVs. Solid lines incorporate shadow costs from fuel subsidies, whereas dashed lines do not.

or about \$1,200 per EV [73]. By comparison, the 10% EV penetration scenario examined in this work corresponds to a fleet of 2.1 million EVs. However, it is important to note that infrastructure and charging costs are highly assumption-dependent. For instance, the aforementioned estimate

includes a share of DC fast chargers, which currently are roughly nine times more expensive than Level-2 chargers [73]. Other infrastructure and system management costs—often specific to local contexts—are excluded from that estimate. Distribution-level studies may use the benchmark values presented here to evaluate the cost-effectiveness of targeted infrastructure investments.

The economic parameters are defined based on cost projections from a moderate technology development scenario. Disruptive technological advancements not considered in this work, especially those in emerging storage technologies, can further enhance the potential of renewable energy generation [49].

Finally, this work presents the significant advantages of flexible EV demand through load shifting, managed charging, and reserves services in an exogenous conventional load. An exogenous load is consistent with the current status of Saudi electricity policies [38]. However, deploying demand-side management programs and energy communities could unlock flexibility benefits for industrial and residential consumers [74].

## 5. Summary and conclusions

This work offers a methodology to analyze the potential impact of EVs and CCS on the generation and transmission capacity expansion planning of a power system with tight emission targets. A deterministic optimization framework with hourly resolution balances interactions between demand, renewable generation technologies, fossil-based units, storage units, internodal transmission, carbon capture facilities, and EVs with and without managed charging.

The effect of climate change on both the supply and demand of electricity

is incorporated and the optimization problem is made tractable through spatial and temporal clustering while preserving low-probability events.

A case study of Saudi Arabia in 2040 with an emission target of 100 million ton of CO<sub>2</sub> is evaluated, considering lifecycle emissions, and projected costs and efficiency parameters.

Initially, we demonstrate that without carbon capture or EVs, an annual cost of 44 billion USD, equivalent to 4% of Saudi Arabia's GDP in 2024, is required to meet the 2040 emissions target. Under current domestic fuel prices, carbon capture reduces the annual costs by 39%. However, domestic fuel subsidies significantly distort the competitiveness of systems with carbon capture, whose shadow costs increase the initially estimated annual costs by 35%. However, a power system with carbon capture is still 18% more economical than without it. Two factors hinder the cost-competitive deployment of renewables beyond 29% capacity share in the presence of carbon capture: i) the lack of renewable resources for balancing the abundant solar power, and ii) the high costs of battery energy storage (BES). A sensitivity analysis of BES costs shows these need to fall below 36% of their projected values to make renewable generation more competitive against carbon capture.

This work also details how EVs—even without further cost reductions in BES—complement energy systems with and without carbon capture, reshaping power system dynamics and potentially closing the gap between them. Adopting EVs as a mitigation strategy—by avoiding tailpipe emissions from conventional passenger vehicles—creates more room for CCGT in the power system, reducing costs and improving abatement efficiency. For instance, annual savings from a 10% uncontrolled EV share are estimated at around \$4,900 per EV in a case that excludes carbon capture. The estimated ben-

efit is much lower in cases that include carbon capture, reaching \$400 per EV. These values provide a budgetary benchmark for infrastructure and incentive investments in electrification.

The synergy between EVs and the power sector increases with managed charging, enhancing renewable generation's cost competitiveness and promoting more efficient utilization of CCGT units. Consequently, managed charging reduces power system costs by six additional percentage points for systems with and without carbon capture. Hence, savings per EV grow 2.5 times larger for a case with carbon capture, reaching approximately \$1,100 per EV. Whereas savings from EVs with managed charging amount to around \$6,500 per EV for a scenario without carbon capture.

Of the three features evaluated for managed charging, load shifting and vehicle-to-grid (V2G) contribute equally to unlocking its economic benefits. The third feature, reserve services from EVs, becomes relevant only in cases with carbon capture, where EVs substitute idle CCGT units during the summer peak. In this case, the savings from reserve services account for 7% of the total impact of managed charging.

We finally demonstrate that if the effect of EVs is included and the shadow costs of fuel subsidies are considered, a power system without carbon capture can result in comparable costs, or even more economical, than those with it.

Our findings emphasize the importance of integrating strategies between the power and transportation sectors to maximize environmental benefits at the lowest cost.

## Acknowledgments

This work was supported by research funding from KAUST and computational resources from the Supercomputing Laboratory from KAUST Core Labs.

## References

- [1] International Energy Agency (IEA), Carbon Emissions in 2022, Technical Report, 2022. URL: [www.iea.org](http://www.iea.org).
- [2] M. Alraddadi, A. J. Conejo, R. M. Lima, Expansion Planning for Renewable Integration in Power System of Regions with Very High Solar Irradiation, *Journal of Modern Power Systems and Clean Energy* 9 (2021) 485–494. doi:10.35833/MPCE.2019.000112.
- [3] International Energy Agency (IEA), Global EV Outlook 2023: Catching up with climate ambitions, Technical Report, 2023. URL: [www.iea.org](http://www.iea.org).
- [4] R. Sioshansi, P. Denholm, The Value of Plug-In Hybrid Electric Vehicles as Grid Resources, *The Energy Journal* 31 (2010) 1–23.
- [5] A. M. Elshurafa, N. Peerbocus, Electric vehicle deployment and carbon emissions in Saudi Arabia: A power system perspective, *Electricity Journal* 33 (2020). doi:10.1016/j.tej.2020.106774.
- [6] R. Sioshansi, P. Denholm, The value of concentrating solar power and thermal energy storage, *IEEE Transactions on Sustainable Energy* 1 (2010) 173–183. doi:10.1109/TSTE.2010.2052078.

- [7] D. Zeng, Y. Dong, H. Cao, Y. Li, J. Wang, Z. Li, M. Z. Hauschild, Are the electric vehicles more sustainable than the conventional ones? Influences of the assumptions and modeling approaches in the case of typical cars in China, *Resources, Conservation and Recycling* 167 (2020). doi:10.1016/j.resconrec.2020.105210.
- [8] G. Puig-Samper Naranjo, D. Bolonio, M. F. Ortega, M.-J. García-Martínez, Comparative life cycle assessment of conventional, electric and hybrid passenger vehicles in Spain, *Journal of Cleaner Production* 291 (2021). doi:10.1016/j.jclepro.2021.125883.
- [9] M. Erans, E. S. Sanz-Pérez, D. P. Hanak, Z. Clulow, D. M. Reiner, G. A. Mutch, Direct air capture: process technology, techno-economic and socio-political challenges, *Energy & Environmental Science* 15 (2022) 1360–1405. doi:10.1039/D1EE03523A.
- [10] S. Hughes, A. Zoelle, M. Woods, S. Henry, S. Homsy, S. Pidaparti, N. Kuehn, H. Hoffman, K. Forrest, A. Sheriff, T. Fout, W. Summers, S. Herron, Cost of Capturing CO<sub>2</sub> from Industrial Sources, Technical Report, National Energy Technology Laboratory - In-house Research, 2022. doi:10.2172/1887586.
- [11] M. Binsted, E. Lochner, J. Edmonds, J. Benitez, J. Bistline, M. Browning, F. D. L. Chesnaye, J. Fuhrman, L. Göke, G. Iyer, K. Kennedy, P. Kyle, C. Lenox, H. McJeon, K. O'Keefe, P. O'Rourke, A. Prabhu, R. Sands, L. Sarmiento, S. Showalter, N. Victor, F. Wood, S. Yu, M. Yuan, Carbon management technology pathways for reaching a U.S. Economy-Wide net-Zero emissions goal, *Energy and Climate Change* 5 (2024) 100154. doi:10.1016/J.EGYCC.2024.100154.

- [12] H. Wang, W. Chen, H. Zhang, N. Li, Modeling of power sector decarbonization in China: comparisons of early and delayed mitigation towards 2-degree target, *Climatic Change* 162 (2020) 1843–1856. doi:10.1007/S10584-019-02485-8/FIGURES/5.
- [13] S. Feron, R. R. Cordero, A. Damiani, R. B. Jackson, Climate change extremes and photovoltaic power output, *Nature Sustainability* 2020 4:3 4 (2020) 270–276. doi:10.1038/s41893-020-00643-w.
- [14] J. I. Mikayilov, A. Darandary, R. Alyamani, F. J. Hasanov, H. Alatawi, Regional heterogeneous drivers of electricity demand in Saudi Arabia: Modeling regional residential electricity demand, *Energy Policy* 146 (2020). doi:10.1016/j.enpol.2020.111796.
- [15] IPCC Sixth Assessment Report Working Group 1: The Physical Science Basis, Summary for Policymakers, in: *Climate Change 2021 – The Physical Science Basis*, Cambridge University Press, 2023, pp. 3–32. doi:10.1017/9781009157896.001.
- [16] M. Hoffmann, L. Kotzur, D. Stolten, M. Robinius, A review on time series aggregation methods for energy system models, *Energies* 13 (2020). doi:10.3390/en13030641.
- [17] F. Souayfane, R. M. Lima, H. Dahrouj, H. P. Dasari, I. Hoteit, O. Knio, On the behavior of renewable energy systems in buildings of three Saudi cities: Winter variabilities and extremes are critical, *Journal of Building Engineering* 70 (2023). doi:10.1016/j.jobe.2023.106408.
- [18] A. T. Perera, V. M. Nik, D. Chen, J. L. Scartezzini, T. Hong, Quantifying the impacts of climate change and extreme climate events

- on energy systems, *Nature Energy* 5 (2020) 150–159. doi:10.1038/s41560-020-0558-0.
- [19] N. E. Koltsaklis, A. S. Dagoumas, State-of-the-art generation expansion planning: A review, *Applied Energy* 230 (2018) 563–589. doi:10.1016/j.apenergy.2018.08.087.
- [20] M. B. Anwar, M. Muratori, P. Jadun, E. Hale, B. Bush, P. Denholm, O. Ma, K. Podkaminer, Assessing the value of electric vehicle managed charging: a review of methodologies and results, This journal is Cite this: *Energy Environ. Sci* 15 (2022) 466. doi:10.1039/d1ee02206g.
- [21] D.-I. Y. Scholz, I. U. Wagner, Renewable energy based electricity supply at low costs-Development of the REMix model and application for Europe, Ph.D. thesis, Stuttgart University, 2012.
- [22] B. Van Der Zwaan, I. Keppo, F. Johnsson, How to decarbonize the transport sector? *Energy Policy*, *Energy Policy* 61 (2013) 562–573. doi:10.1016/j.enpol.2013.05.118.
- [23] M. Carrión, R. Domínguez, R. Zárate-Miñano, Influence of the controllability of electric vehicles on generation and storage capacity expansion decisions, *Energy* 189 (2019). doi:10.1016/j.energy.2019.116156.
- [24] M. Victoria, K. Zhu, T. Brown, G. B. Andresen, M. Greiner, Early decarbonisation of the European energy system pays off, *Nature Communications* 2020 11:1 11 (2020) 1–9. URL: <https://www.nature.com/articles/s41467-020-20015-4>. doi:10.1038/s41467-020-20015-4.
- [25] O. J. Guerra, D. A. Tejada, G. V. Reklaitis, Climate change impacts and adaptation strategies for a hydro-dominated power system

- via stochastic optimization, *Applied Energy* 233-234 (2019) 584–598. doi:10.1016/J.APENERGY.2018.10.045.
- [26] W. Matar, N. Y. Mansouri, E. Umeozor, Energy policy pathways to inform climate policy in Saudi Arabia, *Journal of Cleaner Production* 445 (2024) 141190. doi:10.1016/J.JCLEPRO.2024.141190.
- [27] M. Victoria, K. Zhu, T. Brown, G. B. Andresen, M. Greiner, The role of storage technologies throughout the decarbonisation of the sector-coupled European energy system, *Energy Conversion and Management* 201 (2019) 111977. doi:10.1016/J.ENCONMAN.2019.111977.
- [28] T. Brown, D. Schlachtberger, A. Kies, S. Schramm, M. Greiner, Synergies of sector coupling and transmission reinforcement in a cost-optimised, highly renewable European energy system, *Energy* 160 (2018) 720–739. doi:10.1016/J.ENERGY.2018.06.222.
- [29] C. Li, I. E. Grossmann, A Review of Stochastic Programming Methods for Optimization of Process Systems Under Uncertainty, *Frontiers in Chemical Engineering* 2 (2021). doi:10.3389/fceng.2020.622241.
- [30] B. R. Paudyal, A. G. Imenes, Investigation of temperature coefficients of PV modules through field measured data, *Solar Energy* 224 (2021) 425–439. doi:10.1016/J.SOLENER.2021.06.013.
- [31] F. Pedregosa, V. Michel, O. Grisel, M. Blondel, P. Prettenhofer, R. Weiss, J. Vanderplas, D. Cournapeau, F. Pedregosa, G. Varoquaux, A. Gramfort, B. Thirion, O. Grisel, V. Dubourg, A. Passos, M. Brucher, M. Perrot, E. Duchesnay, Scikit-learn: Machine Learning in Python,

- Journal of Machine Learning Research 12 (2011) 2825–2830. URL:  
<http://scikit-learn.sourceforge.net>.
- [32] R. Stull, Meteorology for Scientists and Engineers, 3rd ed., Earth Science Series, Brooks/Cole, 2015.
  - [33] R. Steadman, The Assessment of Sultriness. Part I: A Temperature-Humidity Index Based on Human Physiology and Clothing Science, Journal of Applied Meteorology and Climatology 18 (1979) 861–873. URL: [https://journals.ametsoc.org/view/journals/apme/18/7/1520-0450\\_1979\\_018\\_0861\\_taosp1\\_2\\_0\\_co\\_2.xml](https://journals.ametsoc.org/view/journals/apme/18/7/1520-0450_1979_018_0861_taosp1_2_0_co_2.xml).
  - [34] E. Zorita, H. Von Storch, The Analog Method as a Simple Statistical Downscaling Technique: Comparison with More Complicated Methods, Journal of Climate 12 (1999). URL: [https://journals.ametsoc.org/view/journals/clim/12/8/1520-0442\\_1999\\_012\\_2474\\_tamaas\\_2.0.co\\_2.xml](https://journals.ametsoc.org/view/journals/clim/12/8/1520-0442_1999_012_2474_tamaas_2.0.co_2.xml).
  - [35] N. Blair, A. Dobos, J. Freeman, T. Neises, M. Wagner, T. Ferguson, P. Gilman, S. Janzou, System Advisor Model, SAM 2014.1.14: General Description., Technical Report NREL/TP-6A20-61019, National Renewable Energy Laboratory, Golden, CO, 2014.
  - [36] National Renewable Energy Laboratory, System Advisor Model<sup>TM</sup> (Computer Program), 2024. URL: <https://sam.nrel.gov>.
  - [37] E. Peterson, J. Hennessey, On the Use of Power Laws for Estimates of Wind Power Potential, Journal of Applied Meteorology and Climatology 17 (1978) 390–394.

- [38] Water and Electricity Regulatory Authority, Annual Statistical Booklet for Electricity Electricity Generation 2022, Technical Report, 2022.
- [39] International Energy Agency (IEA), Saudi Arabia - Emissions - CO2 emissions by sector, 2021, Technical Report, 2022.
- [40] P. Kamboj, M. Hejazi, Y. Qiu, P. Kyle, G. Iyer, The path to 2060: Saudi Arabia's long-term pathway for GHG emission reduction, Energy Strategy Reviews 55 (2024) 101537. doi:<https://doi.org/10.1016/j.esr.2024.101537>.
- [41] J. Krane, W. S. Wilson, Energy Governance in Saudi Arabia: An Assessment of The Kingdom's resources, Policies, and Climate Approach, Technical Report, Rice University's Baker Institute for Public Policy, 2019.
- [42] Saudi Public Investment Fund (PIF) Portfolio, Electric Vehicle Infrastructure Company (EVIQ), Technical Report, 2024.
- [43] A. Volodire, CNRM-CERFACS CNRM-CM6-1-HR model output prepared for CMIP6 HighResMIP Version 2019/10/24, 2019. doi:10.22033/ESGF/CMIP6.1387.
- [44] K. Riahi, D. P. van Vuuren, E. Kriegler, J. Edmonds, B. C. O'Neill, S. Fujimori, N. Bauer, K. Calvin, R. Dellink, O. Fricko, W. Lutz, A. Popp, J. C. Cuaresma, S. KC, M. Leimbach, L. Jiang, T. Kram, S. Rao, J. Emmerling, K. Ebi, T. Hasegawa, P. Havlik, F. Humpenöder, L. A. Da Silva, S. Smith, E. Stehfest, V. Bosetti, J. Eom, D. Gerenaat, T. Masui, J. Rogelj, J. Strefler, L. Drouet, V. Krey, G. Luderer, M. Harmsen, K. Takahashi, L. Baumstark, J. C. Doelman,

- M. Kainuma, Z. Klimont, G. Marangoni, H. Lotze-Campen, M. Obersteiner, A. Tabeau, M. Tavoni, The Shared Socioeconomic Pathways and their energy, land use, and greenhouse gas emissions implications: An overview, *Global Environmental Change* 42 (2017) 153–168. doi:10.1016/J.GLOENVCHA.2016.05.009.
- [45] J. Mikayilov, R. Alyamani, A. Darandary, M. Javid, F. Hasanov, Modeling and Forecasting Industrial Electricity Demand for Saudi Arabia: Uncovering Regional Characteristics, Technical Report, King Abdullah Petroleum Studies and Research Center, Riyadh, 2022. doi:10.30573/KS--2021-DP22.
- [46] D. Fontecha, Modelling Pricing Policies on the Power Sector of Saudi Arabia under the Scope of Vision 2030, MSc. Thesis, KAUST (2022). doi:10.25781/KAUST-H1F7A.
- [47] M. Sengupta, Y. Xie, A. Lopez, A. Habte, G. Maclaurin, J. Shelby, The National Solar Radiation Data Base (NSRDB), *Renewable and Sustainable Energy Reviews* 89 (2018) 51–60. doi:<https://doi.org/10.1016/j.rser.2018.03.003>.
- [48] H. Marouani, Y. Fouad, H. Mrad, A techno-economic assessment and optimization of Dumat Al-Jandal wind farm in Kingdom of Saudi Arabia, *Energy Science & Engineering* 11 (2023) 4398–4407. doi:<https://doi.org/10.1002/ese3.1602>.
- [49] National Renewable Energy Laboratory, 2024 Annual Technology Baseline, 2024. URL: <https://atb.nrel.gov/>.
- [50] US Environmental Protection Agency, Center for Corporate Climate

Leadership, Emission Factors for Greenhouse Gas Inventories, Technical Report, 2014. URL: <http://www.epa.gov/ghgreporting/reporters/subpart/c.html>.

- [51] J. Das, A. U. Rehman, R. Verma, G. Gulen, M. H. Young, Comparative Life-Cycle Assessment of Electricity-Generation Technologies: West Texas Case Study, Energies 17(5) (2024). doi:10.3390/en17050992.
- [52] ARAMCO, Climate change and the energy transition - Sustainability Report, Technical Report, 2023.
- [53] E. Smith, The Cost of CO<sub>2</sub> Transport and Storage in Global Integrated Assessment Modeling, Ph.D. thesis, Massachusetts institute of technology, 2021.
- [54] US Energy Information Administrator, US Natural Gas Electric Power Price, Technical Report, 2024.
- [55] P. Kurup, S. Akar, S. Glynn, C. Augustine, P. Davenport, Cost Update: Commercial and Advanced Heliostat Collectors, Technical Report, National Renewable Energy Laboratory, 2022. URL: [www.nrel.gov/publications](http://www.nrel.gov/publications).
- [56] Y. Hu, G. Xu, C. Xu, Y. Yang, Thermodynamic analysis and techno-economic evaluation of an integrated natural gas combined cycle (NGCC) power plant with post-combustion CO<sub>2</sub> capture, Applied Thermal Engineering 111 (2017) 308–316. doi:10.1016/J.APPLTHERMALENG.2016.09.094.
- [57] Y. F. Nassar, H. J. El-Khozondar, W. El-Osta, S. Mohammed, M. El-naggar, M. Khaleel, A. Ahmed, A. Alsharif, Carbon footprint and

- energy life cycle assessment of wind energy industry in Libya, Energy Conversion and Management 300 (2024) 117846. doi:10.1016/J.ENCONMAN.2023.117846.
- [58] M. A. Mahmud, S. H. Farjana, Comparative life cycle environmental impact assessment of renewable electricity generation systems: A practical approach towards Europe, North America and Oceania, Renewable Energy 193 (2022) 1106–1120. doi:10.1016/J.RENENE.2022.05.031.
- [59] F. Asdrubali, G. Baldinelli, F. D'Alessandro, F. Scrucca, Life cycle assessment of electricity production from renewable energies: Review and results harmonization, Renewable and Sustainable Energy Reviews 42 (2015) 1113–1122. doi:10.1016/J.RSER.2014.10.082.
- [60] N. Ceccarelli, M. Van Leeuwen, T. Wolf, P. Van Leeuwen, R. Van Der Vaart, W. Maas, A. Ramos, Flexibility of low-CO<sub>2</sub> gas power plants: Integration of the CO<sub>2</sub> capture unit with CCGT operation, in: Energy Procedia, volume 63, Elsevier Ltd, 2014, pp. 1703–1726. doi:10.1016/j.egypro.2014.11.179.
- [61] T. Terlouw, K. Treyer, C. Bauer, M. Mazzotti, Life Cycle Assessment of Direct Air Carbon Capture and Storage with Low-Carbon Energy Sources, Environmental Science and Technology 55 (2021) 11397–11411. doi:10.1021/ACS.EST.1C03263/SUPPL{\\_}FILE/ES1C03263{\\_}SI{\\_}001.PDF.
- [62] S. Deutz, A. Bardow, Life-cycle assessment of an industrial direct air capture process based on temperature–vacuum swing ad-

- sorption, *Nature Energy* 2021 6:2 6 (2021) 203–213. doi:10.1038/s41560-020-00771-9.
- [63] M. Pilotelli, B. Grassi, D. Pasinelli, A. M. Lezzi, Performance analysis of a large TES system connected to a district heating network in Northern Italy, *Energy Reports* 8 (2022) 1092–1106. doi:<https://doi.org/10.1016/j.egyr.2022.07.094>.
- [64] Water and Electricity Regulation Authority (WERA), Annual Statistical Booklet for Electricity Electricity Generation 2020, Technical Report, Water & Electricity Regulation Authority, 2020.
- [65] W. Matar, A. M. Elshurafa, Electricity transmission formulations in multi-sector national planning models: An illustration using the KAPSARC energy model, *Energy Reports* 4 (2018) 328–340. doi:<https://doi.org/10.1016/j.egyr.2018.04.004>.
- [66] Ministry of Transport of Saudi Arabia, Mean average monthly daily traffic Summary Report Saudi, Technical Report, 2018. URL: <https://open.data.gov.sa/en/publishers/687e070e-ebbd-4803-b1cd-e56a25887e77>.
- [67] A. Almutairi, Plug-in electric vehicles and their impact on power generation availability: A real survey-based analysis in Saudi Arabia, *Sustainable Cities and Society* 75 (2021) 103389. doi:10.1016/J.SCS.2021.103389.
- [68] U.S. Department of Transportation, National Household Travel Survey 2009, Technical Report, 2009. URL: <https://nhts.ornl.gov>.

- [69] A. Alemanno, D. Fiorello, A. Martino, G. Pasaoglu, G. Scarella, C. Thiel, C. Zubaryeva, Driving and parking patterns of European car drivers : a mobility survey, Publications Office of the European Union, 2012.
- [70] US Energy Information Administrator, Henry Hub Natural Gas Spot Price (Dollars per Million Btu), Technical Report, 2024.
- [71] International Energy Agency, Global EV Data Explorer - EV Stock share (EU27), 2024. URL: <https://www.iea.org/data-and-statistics/data-tools/global-ev-data-explorer>.
- [72] M. S. Ziegler, J. E. Trancik, Re-examining rates of lithium-ion battery technology improvement and cost decline, *Energy & Environmental Science* 14 (2021) 1635–1651. doi:10.1039/D0EE02681F.
- [73] M. Nicholas, Estimating electric vehicle charging infrastructure costs across major U.S. metropolitan areas, Technical Report, 2019.
- [74] A. Faruqui, R. Hledik, G. Wikler, D. Ghosh, J. Priyjanonda, Bringing Demand-Side Management to the Kingdom of Saudi Arabia Final Report, Technical Report, The Brattle Group, 2011.

## **Supporting Information**

This document presents supplementary material for the manuscript "An optimization framework for integrating electric vehicles and carbon capture: bridging cost gaps via EV deployment", by Daniel Fontechá, Ricardo M. Lima, and Omar Knio.

## Note A. Model Formulation

The mathematical formulation introduced in Section 2.1.2 is herein described in detail.

### *Note A.1. Assumptions*

The following assumptions are made:

- All technologies are deployed at the beginning of the year.
- All costs and technical parameters can be represented linearly.
- The conventional demand and that from uncontrolled EVs are inelastic, regardless of the decisions made over the power and transportation sector configuration.
- Only passenger vehicles are electrified. Other vehicle types for road transportation are not.
- EVs are charged from the grid only.
- EV chargers are available for all EVs when these are parked.
- EV users are willing to leave control of the charge and discharge of the vehicles if a large enough incentive is given.
- There are proper communication facilities to have the effective control of EVs.
- The driving patterns of EVs are exogenous and known in advance to the investment and operation decisions made by the system operator.
- A small number of groups can represent the driving patterns of the aggregate vehicle fleets.
- A limited number of representative days can represent one year of power system operation.

- Battery performance degradation in EVs and stationary storage is insignificant during the model’s time horizon.
- Leaks of captured emissions in the transportation and storage stages are negligible.
- The direct air carbon capture facilities are always operated at full capacity.
- Emission differences between EVs and conventional vehicles in the cradle-to-gate and wheel-to-grave phases of the vehicle’s lifecycle are negligible.
- The radiative forcing from climate change is exogenous to the configuration of the power system modeled.
- Voltage angles in all buses are low enough to approximate the AC transmission system by a linearized DC system.

*Note A.2. Notation*

This subsection describes the notation followed in the mathematical formulation in alphabetic order. All variables in the model are represented in lowercase, while parameters are written in uppercase. Subscripts denote the sets of dependencies, and superscripts are used to distinguish between parameters of a similar nature.

**Sets**

$\mathcal{B}$	Set of nodes, indexed by $b$ and $n$ .
$\mathcal{L}$	Set of transmission lines, indexed by $l$ .
$\mathcal{M}$	Set of representative days, indexed by $m$ and $mp$ .
$\mathcal{T}$	Set of periods, indexed by $t$ and $tp$ .

$\Omega_c^b$	Set of carbon capture technologies located in node $b$ , indexed by $c$ .
$\Omega_i^b$	Set of generation units located in node $b$ , indexed by $i$ .
$\Omega_{iren}^b$	Subset of renewable generation units located in node $b$ , indexed by $i$ .
$\Omega_{ifirm}^b$	Subset of fossil-based, firm generation units located in node $b$ , indexed by $i$ .
$\Omega_j^b$	Set of stationary storage units located in node $b$ , indexed by $j$ .
$\Omega_{jround}^b$	Subset of stationary storage units that can return power to the grid, located in node $b$ , indexed by $j$ .
$\Omega_v^b$	Set of vehicle group defined by its driving pattern and located in node $b$ , indexed by $v$ .
$\Omega_k^b$	Set of road types classified by maximum speed limit located in node $b$ , indexed by $k$ .

### Binary variable

$x_{l,b,n}^l$ :	Defines whether transmission line number $l$ between node $b$ and node $n$ is installed ( $x_{l,b}^l = 1$ ) or not ( $x_{l,b}^l = 0$ ).
-----------------	-----------------------------------------------------------------------------------------------------------------------------------------

### Free continuous variable

$a_{b,m,t}$	Voltage angle in node $b$ and period $t$ of representative day $m$ .
-------------	----------------------------------------------------------------------

### Positive continuous variables

$c_b$	Annual carbon emissions captured by direct air capture in node $b$ .
$e_{j,b,m,t}^s$	Energy stored in storage unit $j$ , in node $b$ and period $t$ of representative day $m$ .

$e_{v,b,m,t}^v$	Energy stored in managed share of vehicle type $v$ , in node $b$ and period $t$ of representative day $m$ .
$f_{l,b,n,m,t}$	Power transmitted through line $l$ from node $b$ to node $n$ in period $t$ of representative day $m$ .
$n_{v,b}^{ev}$	Number of EVs with driving pattern $v$ and in node $b$ . This variable is only active for the analysis of the maximum competitive share of EVs.
$r_{i,b,m,t}^g$	Reserves provided by firm generation unit $i$ in node $b$ and period $t$ of representative day $m$ .
$r_{j,b,m,t}^s$	Reserves provided by storage unit $j$ in node $b$ and period $t$ of representative day $m$ .
$r_{v,b,m,t}^v$	Reserves provided by controlled share of vehicle type $v$ , in node $b$ and period $t$ of representative day $m$ .
$u_{b,m,t}$	Unserved energy in node $b$ and period $t$ of representative day $m$ .
$x_{i,b}^g$	Installed capacity of generation unit $i$ in node $b$ .
$x_{j,b}^s$	Installed capacity of storage unit $j$ in node $b$ .
$y_{i,b,m,t}^g$	Power produced by generation unit $i$ , in node $b$ and period $t$ of representative day $m$ .
$y_{j,b,m,t}^{sc/sd}$	Power consumed (charge, $sc$ ) or produced (discharge, $sd$ ) by storage unit $s$ , in node $b$ and period $t$ of representative day $m$ .
$y_{v,b,m,t}^{vcc/vcd}$	Power consumed (charge, $vcc$ ) or produced (discharge, $vcd$ ) by controlled share of vehicle type $v$ , in node $b$ and period $t$ of representative day $m$ .

$y_{v,b,m,t}^{vuc}$	Power demand from charging the fleet of uncontrolled electric vehicles with driving pattern $v$ , in node $b$ and period $t$ of representative day $m$ .
$z^v$	EV adoption: share of the vehicle fleet with driving pattern $v$ that is composed by EVs. This variable is only active for the analysis of the maximum competitive share of EVs.

### Parameters

$A_{i,b,m,t}$	Capacity factor of generation technology $i$ in node $b$ and period $t$ of representative day $m$ .
$B_{l,b,n}$	Susceptance of transmission line $l$ from node $b$ to node $n$ .
$C^{DAC}$	Cost of capturing one ton of carbon dioxide using direct air capture technology.
$C_i^I$	Annualized investment cost of one power unit of installed capacity of generation technology $i$ .
$C_j^I$	Annualized investment cost of one power unit of installed capacity of stationary storage technology $j$ .
$C_{l,b,n}^I$	Annualized investment cost of transmission line $l$ from node $b$ to node $n$ .
$C_i^O$	Operational cost of generation of one power unit from generation technology $i$ .
$C_j^O$	Operational cost of charging and discharging one power unit using stationary storage technology $j$ .
$C^{UE}$	Cost of unserved energy.
$D_{b,m,t}$	Demand in node $b$ and period $t$ of representative day $m$ .
$D^{dac}$	Power consumed by direct air capture to trap one ton of carbon dioxide.

$D_{v,b,m,t}^{drive}$	Electric power consumed by vehicle group $v$ while driving in node $b$ , and period $t$ of representative day $m$ .
$F_{l,b,n}^{max}$	Transmission capacity of line $l$ from node $b$ to node $n$ .
$G_i$	CO <sub>2</sub> -equivalent greenhouse gases emitted by generation technology $i$ .
$G^{max}$	Maximum permitted annual CO <sub>2</sub> -equivalent greenhouse gases from the power sector.
$\bar{G}^{offset}$	Weighted average of tailpipe emissions from conventional vehicles avoided by including an EV fleet instead.
$K^D$	Reserve factor as a fraction of the total demand.
$R_j$	Technical power to energy ratio limit for stationary storage technologies $j$ .
$RL^{up/down}$	Ramping limit up/down of firm generation technology $i \in \Omega^{ifirm}$ .
$SOC_j^{ini}$	Initial state-of-charge (SoC) of stationary storage technology $j$ .
$SOC_{j/v}^{min/max}$	Minimum/maximum state-of-charge (SoC) of stationary storage technology $j$ or electric vehicle fleet $v$ .
$T$	Number of time periods in the time horizon studied. 8760 (hours/year) in this case.
$V^{tot}$	Total vehicle fleet size in node $b$ .
$X_{iren,b}^{gmax}$	Maximum installable capacity of renewable generation technology indexed by $iren$ for resource availability of node $b$ .
$X_{b,n}^{trans}$	Binary parameter that determines existing lines between nodes $b$ and $n$ .

$X_{v,b}$	Aggregated storage capacity of electric vehicle fleet $v$ , in node $b$ .
$Y_{v,b,m,t}^{vuc,unit}$	Power demand from charging one uncontrolled electric vehicle $v$ , in node $b$ and period $t$ of representative day $m$ .
$\xi_v$	Share of electric vehicle fleet with representative driving pattern $v$ .
$\eta^{dac}$	Net carbon abatement efficiency of carbon capture with respect to carbon emission captured
$\eta_{j/v}^{c/d}$	Charging/discharging efficiency of stationary storage technology $j$ or electric vehicle fleet $v$ .
$\psi_v^{ctr}$	Share of electric vehicle fleet $v$ that is controlled.
$\rho_{v,t}^{plug}$	Binary parameter that determines if EV fleet with driving pattern $v$ is plugged to the grid in time period $t$ .
$\theta_m, \theta_t$	Weight of representative day $m$ or period $t$ .

#### Note A.3. Equations

In this section, the equations for the objective function and constraints are listed.

*Note A.3.1. Objective function*

The objective function of the problem minimizes the total cost of investment and operation of the power system,

$$\begin{aligned} \min_{\Phi} & \left[ \sum_{b \in \mathcal{B}} \left( \sum_{i \in \Omega_b^i} C_i^I x_{i,b}^g + \sum_{j \in \Omega_b^j} C_j^I x_{j,b}^s + C^{DAC} c_b + C_{l,b,n}^I x_{l,b,n}^l \right. \right. \\ & \left. \left. + \sum_{m \in \mathcal{M}} \theta_m \sum_{t \in \mathcal{T}} \theta_t \left( \sum_{i \in \Omega_b^i} C_i^O y_{i,b,m,t}^g + \sum_{j \in \Omega_b^j} C_j^O y_{j,b,m,t}^{sc} + C^{UE} u_{b,m,t} \right) \right) \right], \end{aligned} \quad (\text{S1})$$

where  $\Phi$  represents the set of all variables. The objective function is expressed in two lines. The terms in the first line compile the cost of investment in the capacity of generation, stationary storage, direct air capture, and new transmission in that order. The second line introduces the operation costs of generation, cycling stationary storage units (represented by their charging phase), and unserved energy. The parameter  $\theta_m$  incorporates the weights obtained during temporal clustering.

*Note A.3.2. Constraints*

*General balances:.* The emission constraint

$$\begin{aligned} \sum_{m \in \mathcal{M}} \theta_m \sum_{t \in \mathcal{T}} \theta_t \sum_{b \in \mathcal{B}} \left( \sum_{i \in \Omega_b^i} G_i y_{i,b,m,t}^g - \sum_{v \in \Omega_b^v} n_{v,b}^{ev} \bar{G}^{offset} D_{v,b,m,t}^{drive} \right) \\ - \frac{c_b}{T} (1 - \eta^{dac}) \leq G^{max}, \quad \forall w \end{aligned} \quad (\text{S2})$$

sets an upper limit to the net emissions of the system evaluated. The left-hand side of the balance first calculates the weighted average of total emissions from generation. Then, it subtracts two offset alternatives: i) the

tailpipe emissions avoided by using EVs instead of conventional vehicles, and ii) the net carbon abatement effect of direct air capture.

The load balance is ensured at all times with

$$\begin{aligned}
& \sum_{(i \in \Omega_b^i) \neq cspf} y_{i,b,m,t}^g + y_{j=bes,b,m,t}^{sd} \\
& + \sum_{(l \in \mathcal{L})} \sum_{(b \neq n \in \mathcal{B})} (f_{l,n,b,m,t} - f_{l,b,n,m,t}) \\
& + \sum_{v \in \Omega_b^v} y_{v,b,m,t}^{vcd} + u_{b,m,t} \\
& = D_{b,m,t} + \sum_{j \in \Omega_b^j} y_{j,b,m,t}^{sc} + D^{dac} \frac{c_b}{T} \\
& + \sum_{v \in \Omega_b^v} (y_{v,b,m,t}^{vuc} + y_{v,b,m,t}^{vcc}), \quad \forall b, m, t,
\end{aligned} \tag{S3}$$

where the first line represents power deposited by generation and stationary storage units. The second line represents the net power output by transmission lines from the reference node. The third line includes the power discharged from electric vehicles through V2G facilities and the unserved energy. The fourth line formulates the base demand, the power consumed through BES charging and the power consumed by direct air capture. Finally, the fifth line expresses the power demand from charging EVs with (controlled) and without (uncontrolled) managed charging. Note that the stationary storage system integrated in CSP is not included in the constraint S3 given that this system only discharges its thermal energy to the power train of the same technology.

The constraint

$$\begin{aligned} & \sum_{i \in \Omega^{firm}} r_{i,b,m,t}^g + \sum_j r_{j,b,m,t}^s + \sum_v r_{v,b,m,t}^v \\ & \geq K^D \left( D_{b,m,t} + \sum_j y_{j,b,m,t}^{sc} \right. \\ & \quad \left. + \sum_v (y_{v,b,m,t}^{vcc} + y_{v,b,m,t}^{vuc}) \right), \quad \forall b, m, t \end{aligned} \quad (\text{S4})$$

ensures that the reserves available from generation, stationary storage, and EVs with managed charging are always larger than the minimum reserves, determined by the total demand, excluding transmission.

The total installed capacity of new renewable generation units is constrained by the land coverage of the candidate area in capacity terms, given by

$$x_{i,b}^g \leq X_{iren,b}^{gmax}, \quad \forall i \in \Omega_b^{iren}, b, y. \quad (\text{S5})$$

Whereas the generation and reserves are limited by the availability (capacity factor) from generation technologies with constraints

$$y_{i,b,m,t}^g + r_{i,b,m,t}^g \leq A_{i,b,m,t} x_{i,b}^g, \quad \forall i \in \Omega_b^i, b, m, t. \quad (\text{S6})$$

*Ramping limits:*. The intraday ramping limits of firm generation are formulated in

$$y_{i,b,m,t}^g - y_{i,b,m,t-1}^g \leq RL_i^{up} x_{i,b}^g, \quad \forall i \in \Omega^{firm}, b, m, t > t_1, \quad (\text{S7})$$

and

$$y_{i,b,m,t}^g - y_{i,b,m,t-1}^g \geq RL_i^{down} x_{i,b}^g, \quad \forall i \in \Omega^{firm}, b, m, t > t_1. \quad (\text{S8})$$

While the ramping limit adjustments between consecutive representative days is given by

$$y_{i,b,m,t_1}^g - y_{i,b,m-1,t_f}^g \leq RL_i^{up} x_{i,b}^g, \quad \forall i \in \Omega^{ifirm}, b, m > m_1, \quad (\text{S9})$$

and

$$\begin{aligned} y_{i,b,m-1,t_f}^g - y_{i,b,m,t_1}^g &\leq RL_i^{down} x_{i,b}^g, \\ \forall i \in \Omega^{ifirm}, b, m &> m_1. \end{aligned} \quad (\text{S10})$$

*Transmission:.* Constraints (S11)-(S16) represent an altered Big-M approach for the linearized approximation of AC transmission and are a simplified version of the formulation of Guerra et al. [1]. The electricity flow in transmission lines is determined by the susceptance and the voltage angle difference between the connected buses, as established in

$$\begin{aligned} -\frac{\pi}{2} B_{l,b,n} (1 - x_{l,b,n}^l) &\leq f_{l,b,n,m,t} - B_{l,b,n} (a_{b,m,t} - a_{n,m,t}), \\ \forall l, b &\neq n, m, t, \end{aligned} \quad (\text{S11})$$

and

$$\begin{aligned} f_{l,b,n,m,t} - B_{l,b,n} (a_{b,m,t} - a_{n,m,t}) &\leq \frac{\pi}{2} B_{l,b,n} (1 - x_{l,b,n}^l), \\ \forall l, b &\neq n, m, t. \end{aligned} \quad (\text{S12})$$

The existing transmission lines are identified in

$$x_{l,b,n}^l = X_{b,n}^{trans}, \quad \forall l = l_1, b \neq n, \quad (\text{S13})$$

and the transmission capacity of existing and candidate lines is introduced in

$$-F_{l,b,n}^{max} \leq f_{l,b,n,m,t} \leq F_{l,b,n}^{max}, \quad \forall b \neq n, m, t. \quad (\text{S14})$$

The feasible voltage angles are constrained to low enough values by

$$-\pi/3 \leq a_{b,m,t} \leq \pi/3, \quad \forall b, m, t, \quad (\text{S15})$$

to be consistent with the assumptions behind the AC linearization.

Finally, a reference angle is set to zero in

$$a_{b,m,t} = 0, \quad \forall b = b_{ref}, m, t. \quad (\text{S16})$$

*Stationary storage::* Constraints (S17)-(S26) define stationary storage technologies. The energy balance

$$\begin{aligned} & e_{j,b,m,t}^s - e_{j,b,m,t-1}^s \\ &= y_{j,b,m,t}^{sc} \eta_j^c - \frac{y_{j,b,m,t}^{sd}}{\eta_j^d}, \quad \forall j, b, m, t > t_1 \end{aligned} \quad (\text{S17})$$

makes intraday changes in the energy stored based on the charging and discharging rates. Likewise, the energy balance between consecutive representative days is established by

$$\begin{aligned} & e_{j,b,m,t_1}^s - e_{j,b,m-1,t_f}^s \\ &= y_{j,b,m,t}^{sc} \eta_j^c - \frac{y_{j,b,m,t}^{sd}}{\eta_j^d}, \quad \forall j, b, m > 1, t, \end{aligned} \quad (\text{S18})$$

The energy stored is bounded by the operative states of charge of the stationary storage unit in

$$SOC_j^{min} x_{j,b}^s \leq e_{j,b,m,t}^s \leq SOC_j^{max} x_{j,b}^s, \quad \forall j \in \Omega_j^b, b, m, t. \quad (\text{S19})$$

Moreover, the charging rate is limited by the technical capacities of stationary storage technology in

$$y_{j,b,m,t}^{sc} \leq \frac{x_{j,b}^s}{R_j}, \quad \forall j, b, m, t. \quad (\text{S20})$$

Similarly, the discharging and reserve capacities are limited by the technical capacities of the stationary storage technology in

$$y_{j,b,m,t}^{sd} + r_{j,b,m,t}^s \leq \frac{x_{j,b}^s}{R_j}, \quad \forall j, b, m, t. \quad (\text{S21})$$

Additionally, the discharging and reserve capacities are also constrained by the total energy stored by

$$y_{j,b,m,t}^{sd} + r_{j,b,m,t}^s \leq se_{j,b,m,t}, \quad \forall j, b, m, t. \quad (\text{S22})$$

At the initial period in the time horizon, the constraint

$$y_{j,b,m_1,t_1}^{sc} = 0, \quad \forall j, b, m \quad (\text{S23})$$

sets the charging rate to zero. Whereas

$$y_{j,b,m,t_1}^{sd} = 0, \quad \forall j, b, m \quad (\text{S24})$$

does likewise with the discharging rate. To prevent sharp end-of-horizon effects

$$e_{j,b,y_1,m_1,t_1}^s = SOC^{ini}x_{j,b}^s, \quad \forall j, b, \quad (\text{S25})$$

and

$$e_{j,b,y_f,m_f,t_f}^s = SOC^{ini}x_{j,b}^s, \quad \forall j, b \quad (\text{S26})$$

bound the initial and final stored energy to a given SoC value.

*CSP*: In addition to the stationary storage and generation constraints, the blocks that compose CSP are balanced in

$$\begin{aligned} y_{cspg,b,m,t}^g &\leq y_{cspf,b,m,t}^g \\ &+ y_{cspg,b,m,t}^{sd} - y_{cspg,b,m,t}^{sc}, \quad \forall b, m, t, \end{aligned} \quad (\text{S27})$$

where the power generated from CSP is limited to net the equivalent power available from the solar field after balancing it with the equivalent thermal energy stored. Additionally, the equivalent reserves available from the storage sub-unit of CSP are constrained by the total capacity of the powertrain of CSP, given by

$$y_{csp, b, m, t}^{sd} + r_{csp, b, m, t}^s \leq A_{cspg, b, m, t} x_{cspg, b}^g, \quad \forall b, m, t. \quad (\text{S28})$$

*EVs:* The size of the electric vehicle fleet is determined by

$$n_{v, b}^{ev} = V_y^{tot} \xi_v z_y^v, \quad \forall v, b, \quad (\text{S29})$$

where the parameter  $\xi_v$  classifies the vehicle fleet according to their driving pattern and  $z^v$  represents the share of vehicle fleet that is electrified (EV adoption). The value of  $z^v$  is fixed in the epsilon constraint analysis, which comprises most of this work. However, releasing this variable provides relevant information on to what extent electrification is a competitive decarbonization strategy. The variable  $n_{v, b}^{ev}$  is not explicitly necessary, but it facilitates the readability of this formulation with negligible impact on its performance.

The exogenous charging patterns of uncontrolled vehicles are scaled up to the size of the EV fleet with the corresponding driving patterns in

$$y_{v, b, m, t}^{vuc} = Y_{v, b, m, t}^{vuc, unit} n_{v, b}^{ev}, \quad \forall v, b, m, t. \quad (\text{S30})$$

It is worth noting that  $Y_{v, b, m, t}^{vuc, unit}$  is calculated during pre-processing, balancing the charging stages with the SoC of the EV batteries and factoring by the share of uncontrolled EVs:  $(1 - \psi_v^{ctr})$ .

Analogous to stationary storage technologies, the balance

$$\begin{aligned} e_{v,b,m,t}^v - e_{v,b,m,t-1}^v &= y_{v,b,m,t}^{vcc} \eta_v^c \\ &\quad - \frac{y_{v,b,m,t}^{vcd}}{\eta_v^d} - D_{v,b,m,t}^{drive}, \quad \forall v, b, m, t, \end{aligned} \quad (\text{S31})$$

makes intraday changes in the aggregated energy stored in EVs based on the charging rates and discharging ones caused by V2G or by the utilization of the vehicle. Likewise, the energy balance between consecutive representative days is established by

$$\begin{aligned} e_{v,b,m,t_f}^v - e_{v,b,m-1,t_1}^v &= y_{v,b,m,t}^{vcc} \eta_v^c \\ &\quad - \frac{y_{v,b,m,t}^{vcd}}{\eta_v^d} - D_{v,b,m,t}^{drive}, \quad \forall v, b, m, t. \end{aligned} \quad (\text{S32})$$

The total capacity of the given controlled EV fleet and the preferred SoC range bound the aggregated energy stored in the EV group as defined in

$$SOC_v^{min} X_{v,b} \psi_v^{ctr} \leq e_{v,b,m,t}^v \leq SOC_v^{max} X_{v,b} \psi_v^{ctr}, \quad \forall v, b, m, t. \quad (\text{S33})$$

Moreover, the charging rate is limited by the technical capacities of the EV group in

$$y_{v,b,m,t}^{vcc} \leq n_{v,b}^{ev} CR^{EV} \rho_{v,t}^{plug} \psi_v^{ctr}, \quad \forall v, b, m, t, \quad (\text{S34})$$

where  $\rho_{v,t}^{plug}$  is a binary parameter that defines whether the vehicle is plugged in or not. Similarly, the discharging and reserve capacities are limited by the technical capacities of EV group in

$$y_{v,b,m,t}^{vcd} + r_{v,b,m,t}^v \leq n_{v,b}^{ev} CR^{EV} \rho_{v,t}^{plug} \psi_v^{ctr}, \quad \forall v, b, m, t. \quad (\text{S35})$$

Additionally, the discharging and reserve capacities are also constrained by the total energy stored in the EV groups in

$$y_{v,b,m,t}^{vcd} + r_{v,b,m,t}^v \leq e_{v,b,m,t}^v \psi_v^{ctr}, \quad \forall v, b, m, t. \quad (\text{S36})$$

At the initial period in the time horizon, the constraints

$$y_{v,b,m_1,t_1}^{vcc} = 0, \quad \forall v, b \quad (\text{S37})$$

set the charging rate to zero. Whereas

$$y_{v,b,m_1,t_1}^{vcd} = 0, \quad \forall v, b, m \quad (\text{S38})$$

does likewise with the discharging rate. Ultimately for EV groups and to prevent sharp end-of-horizon effects, the constraints

$$e_{j,b,y_1,m_1,t_1}^v = SOC_v^{ini} X_{v,b} \psi_v^{ctr}, \quad \forall v, b, m, t, \quad (\text{S39})$$

and

$$e_{j,b,y_f,m_f,t_f}^v = SOC_v^{ini} X_{v,b} \psi_v^{ctr}, \quad \forall v, b, m, t, \quad (\text{S40})$$

bound the initial and final aggregated stored energy to a given SoC.

## Note B. Effect of climate change over demand

Supplementary Figures S1 and S2 show the historical [2] and expected effect of climate change [3] in the cooling and heating degree days, respectively. More cooling degree days through time indicate hotter and/or more frequent hot days. Whereas less heating degree days indicate less frequency in the demand for heating to compensate cold days.

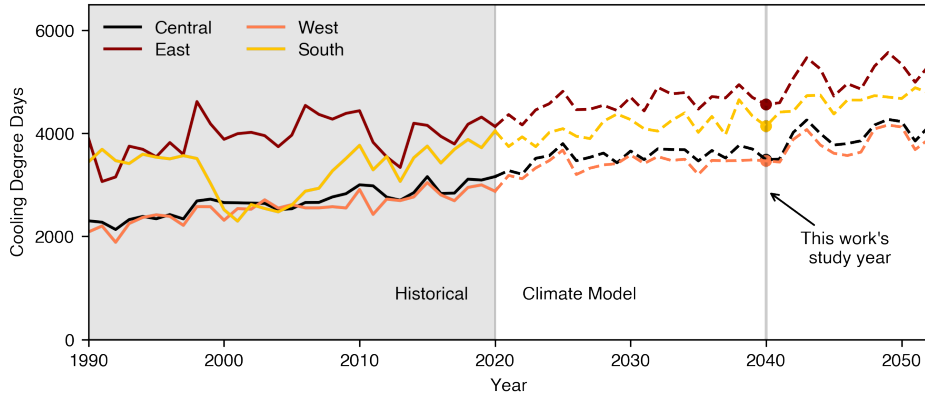


Figure S1: Historical and forecasted cooling degree days ( $^{\circ}\text{F}$ ) for the four nodes of the case study. The calculation is made with the heat index, which adjusts for the humidity effect on the displeasure of individuals.

The totalized demand projection made for the study case is presented in Supplementary Figure S3. The population is assumed to grow at a constant rate of 1.59% [4]. In a scenario accounting for climate change effects since 2020, electricity demand increases to 427 GWh by 2040—5.4% higher than in a scenario without climate change.

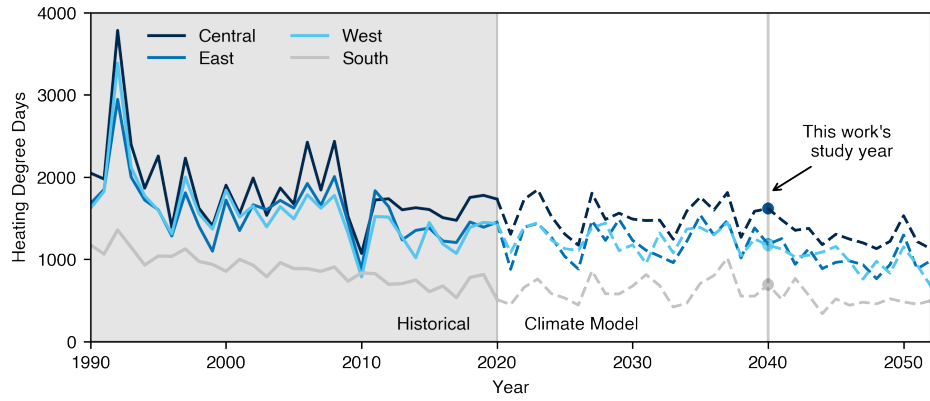


Figure S2: Historical and forecasted heating degree days ( $^{\circ}\text{F}$ ) for the four nodes of the study case. The calculation is made with the heat index, which adjusts for the humidity effect on the displeasure of individuals.

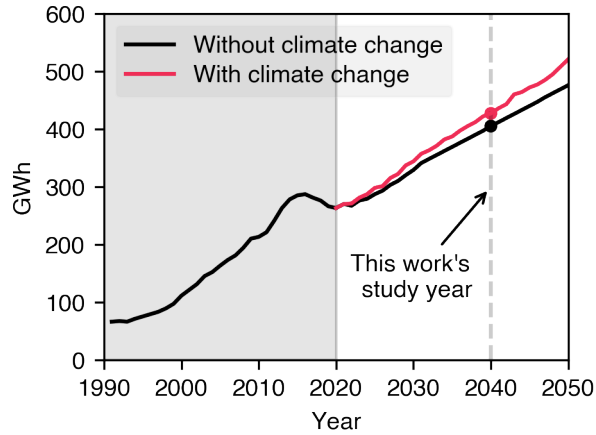


Figure S3: Comparison of total demand projection for the study case (with climate change) and for a case without climate change.

#### Note C. Within cluster sum of squared error (WCSS) analysis and cluster number

Supplementary Figure S4 illustrates how the WCSS falls as the number of clusters grows. The rate at which the error falls stagnates for more than 9

clusters. 10 clusters are selected.

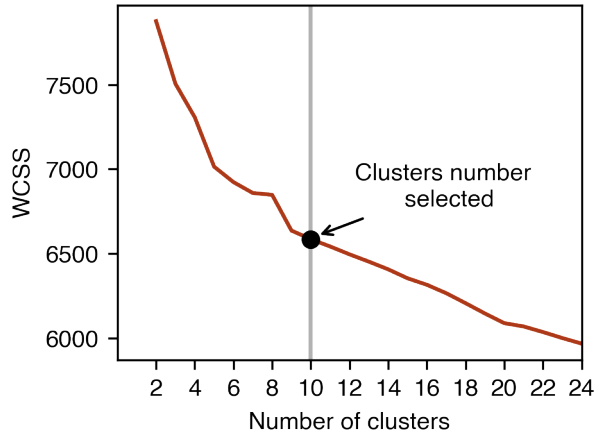


Figure S4: Within cluster sum of squared error (WCSS) to a number of temporal clusters with five fixed spatial clusters per node.

Each technology's total distribution of attribute values was compared before and after the clustering procedure. This method is employed to infer the limitations of the clustering procedure and identify which features are over or underexpressed in the clustered dataset. The dataset for each technology comprises three attributes: shortwave solar radiation, surface temperature, and wind speed.

For instance, Supplementary Figure S5 shows that the solar radiation for PV has an overexpression of radiations close to  $330 \text{ W/m}^2$ , at the expense of underexpression of lower solar radiations. Hence, the clustering procedure somewhat overvalues the total radiation available. Still, values with low solar radiation and probability of occurrence are effectively incorporated in the clustered dataset. Supplementary Figures S6 and S7 provide other representative distributions. In all cases, the clustered dataset approximates the skewed distribution shapes. Although the most extreme values are not

incorporated, low probability values are identified in the clustered datasets.

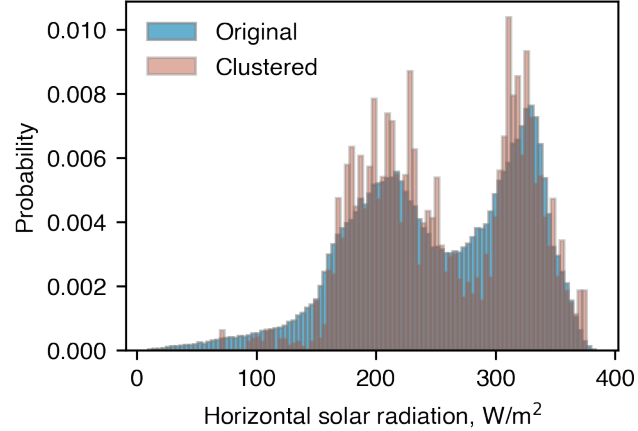


Figure S5: Radiation distribution comparison for solar technology with 10 temporal clusters of 7 consecutive days each, and the partitional k-medoids algorithm.

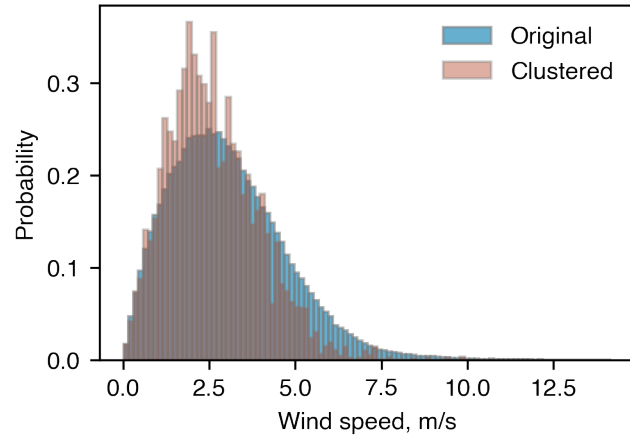


Figure S6: Wind speed distribution comparison for wind turbines with 10 temporal clusters of 7 consecutive days each, and the partitional k-medoids algorithm.

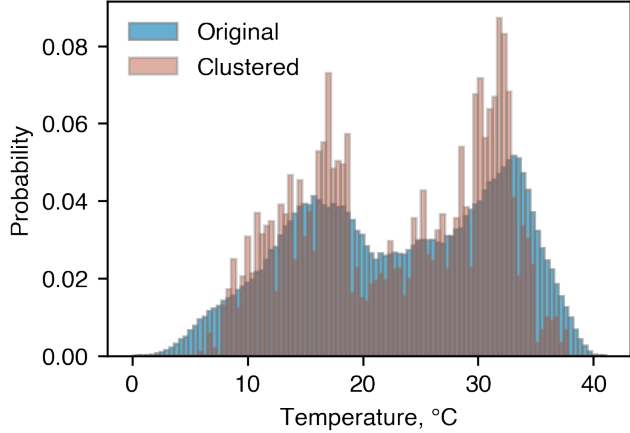


Figure S7: Temperature distribution comparison for CSP technology with 10 temporal clusters of 7 consecutive days each, and the partitional k-medoids algorithm.

#### Note D. Vehicle groups, parameters and traffic data

Each vehicle group is characterized by online and offline periods. The first and second vehicle groups in Table S2 reflect commutes to work, lunch, and back home. The first assumes vehicle chargers are available at work, whereas the second does not. The third and fourth vehicle groups assume operation of vehicles between 9 am and 9 pm for other types of commutes. The fifth group assumes operation overnight, with online times only during the day. The share of each vehicle group was adjusted to fit the total traffic distribution estimated from publicly available consolidated data [5].

Supplementary Figure S8 compares the vehicle distribution estimated from the available data with that of the five representative vehicle groups selected. For each peak hour of the traffic data, a Gaussian distribution is assumed, and then all Gaussian distributions are summarized. Both the total traffic distribution and that of the vehicle groups match the reported

average daily vehicle count of 1.77 million [5].

Table S2: Vehicle aggregator online(shadowed) and offline (white) times and shares.

Vehicle group	Hour of the day																								Share	
	1	2	3	4	5	6	7	8	9	10	11	12	13	14	15	16	17	18	19	20	21	22	23	24		
1																										15.8%
2																										23.8%
3																										19.8%
4																										14.3%
5																										26.4%
																									Total 100%	

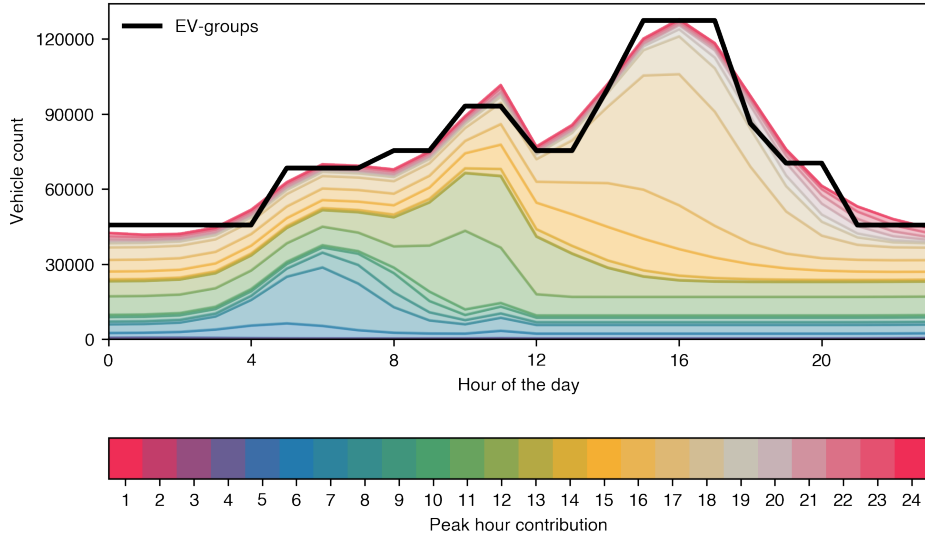


Figure S8: Comparison between vehicle distribution estimated from peak hour vehicle count data from [5] and that of the five vehicle groups defined in this work. The reference vehicle distribution assumes i) a normal distribution with peak time as the mean for each hour of the day and ii) traffic flow in each road that never falls below 10% of its peak level.

The average mileage for each vehicle group in each node is calculated based on assumed average speeds of 80, 120, or 140 km/h, with allocation probabilities of 40%, 30%, and 30%, respectively. These probabilities reflect the distance-weighted distribution of speed limits on the roads within the study area. The results, constrained by the EV battery limitations, derive in an average daily mileage ranging between 80 and 266 km.

Table S3: Technical parameters of vehicles.

	Parameter	Units	Value
General	Passenger vehicle fleet size [6]	million units	20.6
	Commuting time to offline time ratio [5]	h/h	15%
Conventional vehicles	Tailpipe CO <sub>2</sub> emissions [7, 8]	kg/km	0.20
	Energy storage capacity [9]	kWh	72.2
Electric vehicles	Max. charging/discharging rate [10]	kW	15
	Commuting efficiency [9]	kWh/km	0.19
	Charging/discharging efficiency [11]	MWh/MWh	90%
	Maximum SoC	MWh/MWh	95%
	Minimum SoC	MWh/MWh	5%
	Initial/final SoC	MWh/MWh	70%

Other vehicle parameters are incorporated in Table S3. For conventional vehicles, the tailpipe emissions are set to 200 g CO<sub>2</sub>/km, which is between the average emissions for new and existing vehicles in the US with 127.6 and 250 g CO<sub>2</sub>/km, respectively [8]. Meanwhile, technical parameters define the interaction of EVs with the grid. Level 2 chargers constrain the cycling rate of electric vehicles rather than the battery of the vehicle. Consequently, EVs

take around 4.5 hours to fully charge from the minimum to the maximum SoC allowed. The EV charging efficiency is driven by the AC to DC conversion and, to a lesser extent, by the net charging efficiency of EV batteries [11].

### Note E. Pareto fronts for 1% EV adoption

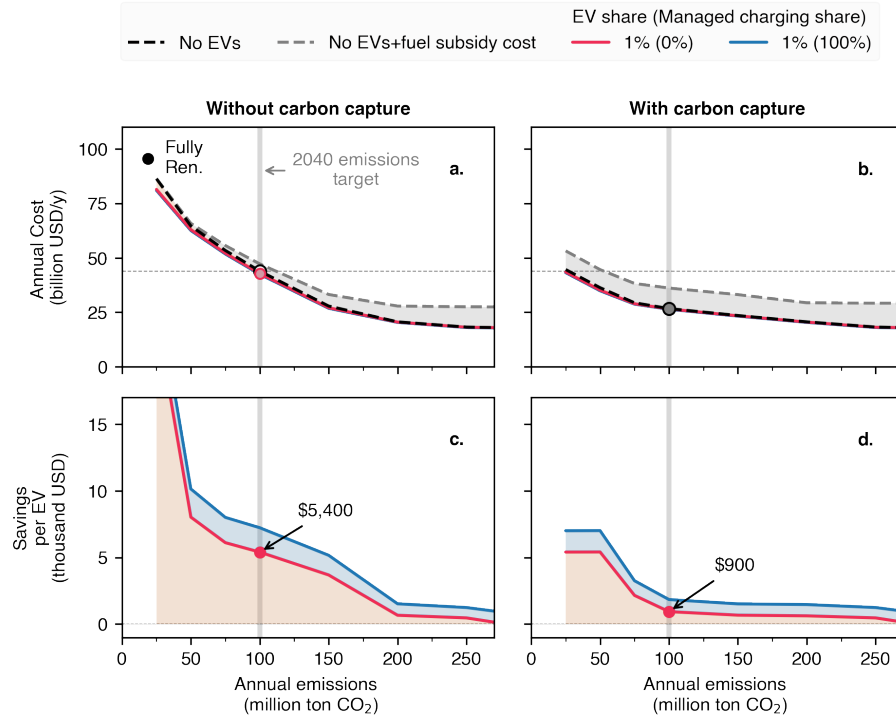


Figure S9: Effect of EVs and carbon capture on annual costs to meet decarbonization targets. Pareto fronts for: a) systems without carbon capture, and b) systems with carbon capture. The dashed black lines represent cases without EVs. Colored lines correspond to a 1% EV adoption share relative to the projected 2040 passenger vehicle fleet, with managed charging levels of 0% (pink) and 100% (blue). Shadow costs from fuel subsidies are included as gray dashed lines. Panels c) and d) show savings per EV for systems without and with carbon capture, respectively.

### Note F. Marginal abatement costs

Supplementary Figure S10 reflects the effect of carbon capture in the marginal abatement cost of a power system, defined as the cost of further reducing emissions by 1 ton of CO<sub>2</sub>. The plot shows an inflection point of 200 million ton of carbon dioxide for systems without carbon capture. It highlights the condition to which wind turbines and BES start to be needed to balance solar power. The inflection point for a case with carbon capture happens

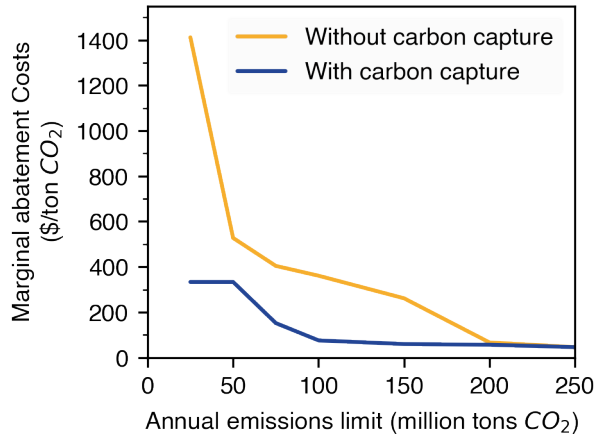


Figure S10: Effect of 10% EV adoption and no managed share in the marginal abatement cost of two decarbonization scenarios.

at 100 million ton of carbon dioxide. At this point, the decarbonization opportunity of point-source carbon capture starts to saturate. Onwards, solar power starts constituting a higher share of the grid. Only then is DAC competitive, as a last-mile decarbonization alternative.

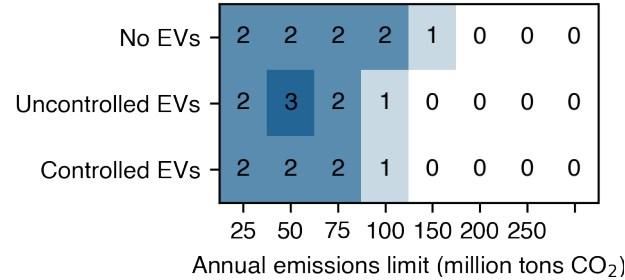


Figure S11: Number of transmission lines built out of 5 candidates for cases without carbon capture.

#### Note G. Transmission profiles

Supplementary Figure S11 presents the number of lines built for each case without carbon capture. The spatial dependence of renewables and the large cost of BES increase the regional interdependence in a system without carbon capture. In contrast, no transmission lines were built in a case with carbon capture. Supplementary Figure S12 compares the role of transmission lines in a case with and without carbon capture. In this case, the West-South transmission line doubles its capacity. Notice also that the Central-West line is more often saturated for a case without carbon capture.

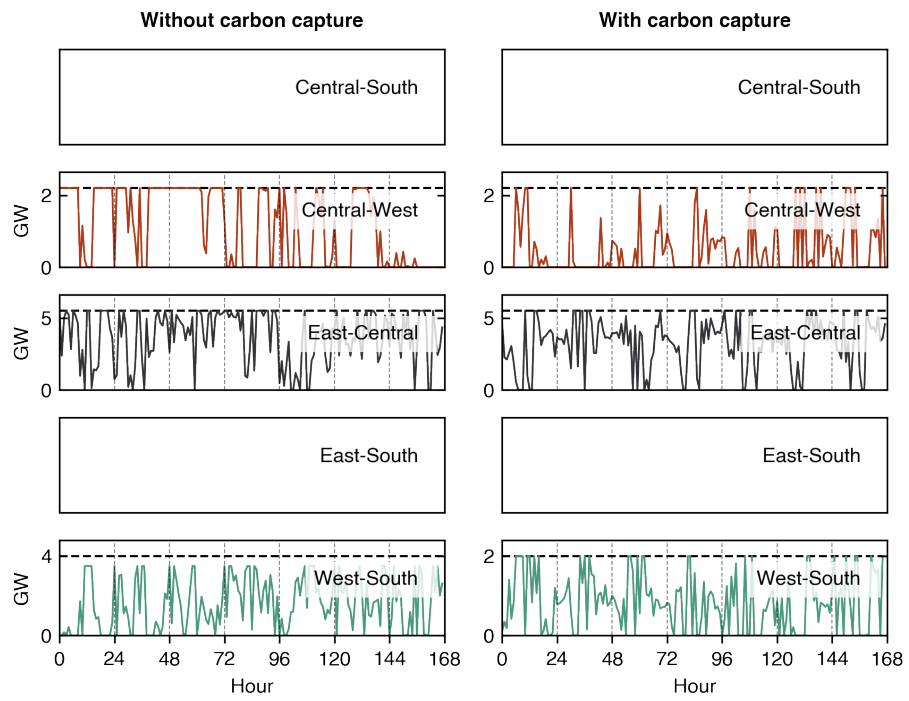


Figure S12: Transmission flow and capacity limits (dashed lines) between nodes for scenario of days 49 to 55, corresponding to a week in September. The cases consider a 10% EV adoption share, 100% share of EVs with managed share, and an annual emission target of 100 million ton of carbon dioxide. Blank plots for null transmission capacity.

## Note H. EV profiles

Supplementary Figure S13 illustrates the charging/discharging patterns of a representative vehicle group. Bars show charging (blue), V2G (red), and reserve services available (black) abiding by the power limit of EV batteries. Periods without bars reflect that EVs are disconnected from the grid. The total energy stored in EV batteries (gray area) remains below their maximum capacity and fluctuates with charging, V2G use, and vehicle use.

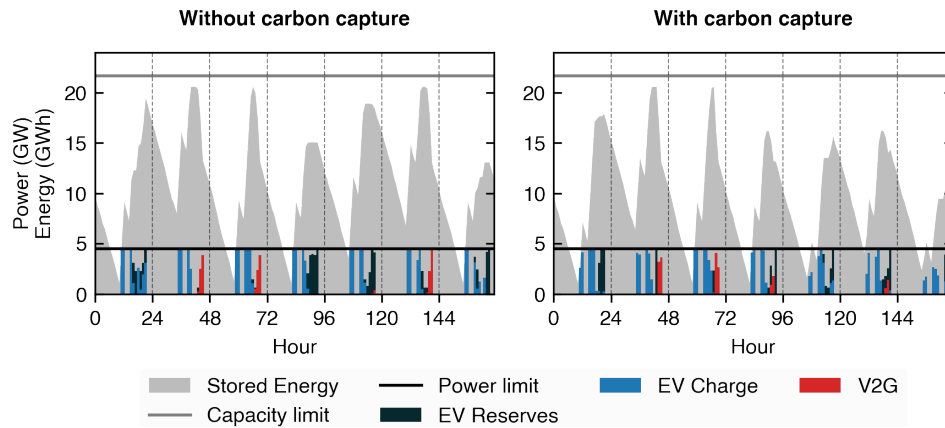


Figure S13: EV battery profiles for vehicle group 4 for days 49 to 55. Bars and black line in power units. Gray area and gray line in energy units.

## References

- [1] Omar J. Guerra, Diego A. Tejada, and Gintaras V. Reklaitis. An optimization framework for the integrated planning of generation and transmission expansion in interconnected power systems. *Applied Energy*, 170:1–21, 5 2016.
- [2] General Authority of Statistic. Historical data of weather stations in Saudi Arabia. Technical report, 2020.
- [3] Aurore Voldoire. CNRM-CERFACS CNRM-CM6-1-HR model output prepared for CMIP6 HighResMIP Version 2019/10/24, 2019.
- [4] Jeyhun I. Mikayilov, Abdulelah Darandary, Ryan Alyamani, Fakhri J. Hasanov, and Hatem Alatawi. Regional heterogeneous drivers of electricity demand in Saudi Arabia: Modeling regional residential electricity demand. *Energy Policy*, 146, 11 2020.
- [5] Ministry of Transport of Saudi Arabia. Mean average monthly daily traffic Summary Report Saudi. Technical report, 4 2018.
- [6] Amro M. Elshurafa and Nawaz Peerbocus. Electric vehicle deployment and carbon emissions in Saudi Arabia: A power system perspective. *Electricity Journal*, 33(6), 7 2020.
- [7] European Environment Agency. Average CO<sub>2</sub> emissions from new cars and new vans increased again in 2019. Technical report, 12 2020.
- [8] U.S. Environmental Protection Agency (EPA), Office of Transportation, Air Quality, and Climate Division. Greenhouse Gas Emissions from a Typical Passenger Vehicle: Questions and Answers – Fact Sheet (EPA-420-F-23-014, June 2023). Technical report, 2023.

- [9] EV Database. Electric Vehicle Database. <https://ev-database.org>, 2024.
- [10] U.S. Department of transportation. Charger Types and Speeds. Technical report, 6 2023.
- [11] Kristian Sevdari, Lisa Calearo, Bjørn Harald Bakken, Peter Bach Andersen, and Mattia Marinelli. Experimental validation of onboard electric vehicle chargers to improve the efficiency of smart charging operation. *Sustainable Energy Technologies and Assessments*, 60:103512, 2023.